Journal of Sound and Vibration (2000) **230**(3), 617–648
doi:10.1006/jsvi.1999.2632, available online at http://www.idealibrary.com on IDEAL®

THE EFFECTS OF VARIOUS DESIGN PARAMETERS ON THE FREE VIBRATION OF DOUBLY CURVED COMPOSITE SANDWICH PANELS

P. R. CUNNINGHAM, R. G. WHITE AND G. S. AGLIETTI

Department of Aeronautics and Astronautics, University of Southampton, Southampton, SO17 1BJ, England

(*Received* 18 *May* 1999, *and in final form* 10 *August* 1999)

Sandwich panels have a very high stiffness to weight ratio, which makes them particularly useful in the aerospace industry where carbon fibre reinforced plastics and lightweight honeycomb cores are being used in the construction of floor panels, fairings and intake barrel panels. In the latter case, the geometry of the panels can be considered doubly curved. This paper presents an introduction to an ongoing study investigating the dynamic response prediction of acoustically excited composite sandwich panels which have double curvature. The final objective is to assess and hopefully produce an up to date set of acoustic fatigue design guidelines for this type of structure. The free vibration of doubly curved composite honeycomb sandwich panels is investigated here, both experimentally and theoretically, the latter using a commerically available finite element package. The design and manufacture of three test panels is covered before presenting experimental results for the natural frequencies of vibration with freely supported boundary conditions. Once validated against the experimental results, the theoretical investigation is extended to study the effects of changing radii of curvature, orthotropic properties of the core, and ply orientation on the natural frequencies of vibration of rectangular panels with various boundary conditions. The results from the parameter studies show curve veering, particularly when studying the effect of changing radii and ply orientation, however, it is not clear whether this phenomenon is due to the approximation method used or occurs in the physical system.

1. INTRODUCTION

Sandwich construction has been favoured for many years where the application dictates the need for a structure with a high stiffness-to-weight ratio. This is particularly true in the aerospace industry where, recently, metallic sandwich structures have been largely superseded by composite constructions employing a mixture of carbon fibre reinforced plastics (CFRP) and foil or paper honeycombs. Typical modern aircraft applications are mainly in secondary structures such as floor panels, fairings, and intake barrel panels and in the latter case, the geometry of the panels can be considered to be doubly curved. The free and forced vibration of flat and singly curved sandwich panels has been investigated by many authors in

0022-460X/00/080617 + 32 $35.00/0

the past [1–5], and a small amount of work has been carried out on sandwich panels with a doubly curved geometry [6, 7]. With the increasing use of CFRP sandwich construction, the need for a set of up to date acoustic fatigue design guidelines becomes apparant, and an examination of the data sheets available [2, 8] has revealed a lack of data for such structures.

This paper presents the results from one phase of a study concerned with the dynamic response of doubly curved composite honeycomb sandwich structures to random acoustic excitation. The intention of this study, which is currently in progress, is to assess and hopefully extend current design methods originally developed by Miles [9], Powell [10], and Clarkson [11], to structures employing composite materials such as CFRP and resin impregnated paper honeycomb. The current acoustic fatigue design processes, which were originally developed for metallic panel-type structures, are based upon prediction of surface strain as a fatigue indicator [2, 11]. For composites, it is the combination of internal stresses/strains within a small critical volume inside the structure which will cause fatigue damage to initiate and propagate [12]. It is therefore worthwhile re-examining the acoustic fatigue design process for advanced composite structures [12], which is the impetus behind the current study. The free vibration of doubly curved, composite honeycomb rectangular sandwich panels is addressed in this paper. The design and manufacture of a set of sandwich panels is discussed by way of an introduction to the programme of work. Results from the initial free vibration experiments are then presented and are used to validate the finite element model which will be used throughout the study. This model is then used to study the effects of various design parameters such as the radii of curvature, the orthotropic properties of the core, and the ply orientation, for three boundary conditions, namely freely supported, simply supported, and fully clamped, on the first four natural frequencies of vibration.

2. DESIGN AND MANUFACTURE OF THE TEST PANELS

A range of experimental test panels with different radii of curvature were designed and manufactured at the University of Southampton. Three panels were designed with various radii of curvature and with identical ply orientation, thickness, plan area, and bevelled edge design. The sandwich lay-up in each case was symmetric with four carbon fibre reinforced plastic layers on either side of the core.

The face plates were made using SP Systems SE84/RC200P/1000/42 epoxy resin pre-impregnated plain weave carbon fibre cloth which was bonded to the core using SP Systems SA80 adhesive film. A lightweight resin impregnated paper honeycomb, namely Hexcel AEROWEB® A1-48-5 OX, was used for the core. Each panel was manufactured using an aluminium alloy mould tool with a convex mould surface to the specified radii of curvature. The panels were cured in a conventional temperature controlled oven which meant a low-temperature curing pre-preg was required.

The panels were designed with a constant plan area of 0·912 m $\times$ 0·525 m to fit the test aperture of the Progressive Wave Tube (PWT) facility at the University of

Southampton, where they will later be tested under random acoustic excitation at sound pressure levels up to 160 dB. Three radii of curvature designs were employed; $R_x = 3{\cdot}5\ \text{m} \times R_y = 1{\cdot}0\ \text{m}$ (Panel #1), $R_x = 1{\cdot}2\ \text{m} \times R_y = 1{\cdot}0\ \text{m}$ (Panel #2), and $R_x = 3{\cdot}5\ \text{m} \times R_y = 0{\cdot}5\ \text{m}$ (Panel #3), with x being the long side dimension and y being the short side dimension.

The panel design can be broken into four main sections; the facing skin which forms the inner face of the panel, the core, the edge pan plies which enclose the edge of the core and form the attachment flange and bevelled edge, and the backing skin which forms the outer face of the panel. This design is typical of that used in the construction of aircraft-type panels such as intake barrel panels and flap fairing panels; a similar design was used by Soovere [1] during his investigation of flat honeycomb sandwich panels.

2.1. BEVELLED EDGE DETAILS

Figure 1 shows the arrangement of the panned down edge, or bevelled edge, which is typical of in-service aircraft honeycomb sandwich panels. The honeycomb was chamfered to an angle of 25° relative to the bottom face on one side along all four edges to form the pan, and edge pan plies being layed up over the honeycomb to totally enclose the core. The use of separate edge pan plies to enclose the core

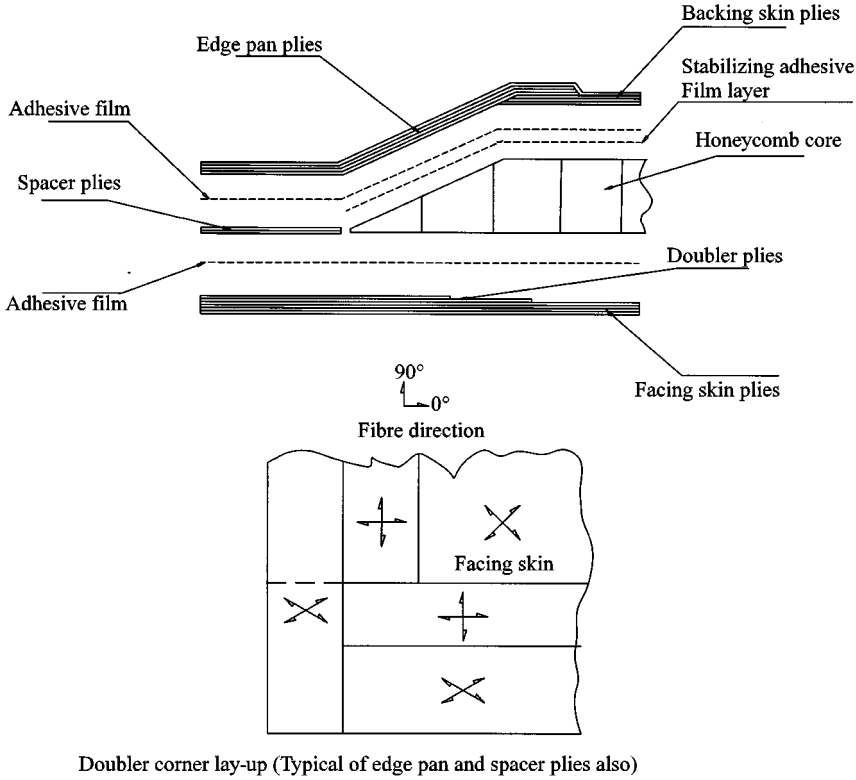

Figure 1. Panel lay-up and bevelled edge detail.

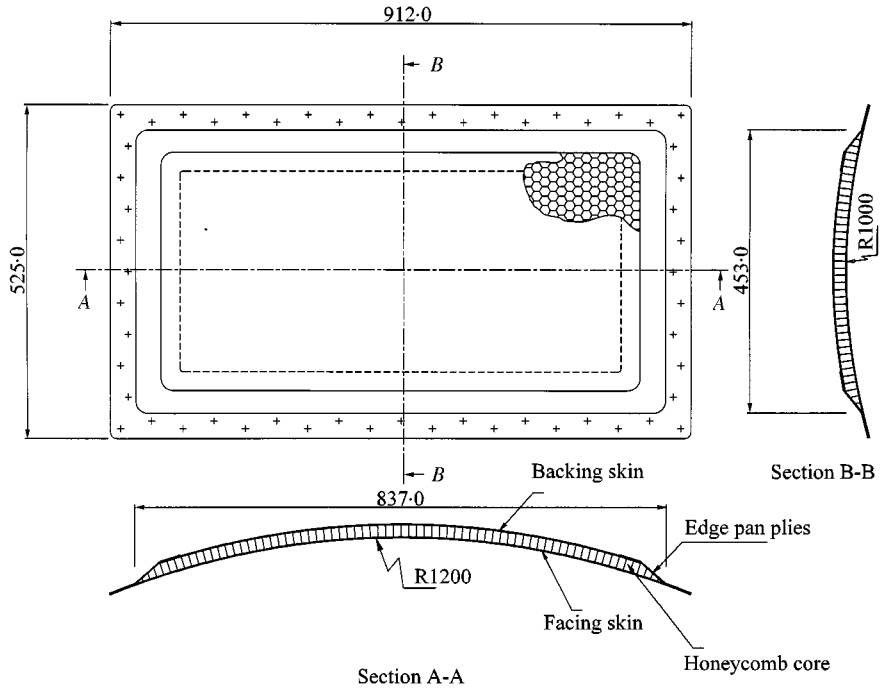

Figure 2. A typical test panel drawing.

avoids excessive wastage of material when forming the backing skin. Doubler plies were incorporated in the layup in order to provide better load transfer in the bevelled edge region, and spacer plies were included in the edge pan to stiffen the attachment flange. In order to provide maximum lap shear and bearing strength, in addition to high panel edge and closeout pan stiffness, 0° and $\pm 30°$ fibre orientations (normal to the panel edge) were used [1]. The backing skin and facing skin plies had fibre orientations of $\pm 45°$ and 0/90°. A typical drawing of one of the test panels is shown in Figure 2.

2.2. LAY-UP PROCEDURE

Before manufacturing a panel, the mould tool was prepared to prevent the resin bonding to the surface of the mould. FREKOTE® B15 sealant and 700C release agent were used for this purpose. The lay-up procedure for each panel, which is shown in Figure 3 and Table 1, was as follows:

Stage 1: facing skin and doubler plies. Cure at 100°C for 4 h, minimum 85% vacuum pressure (650 mmHg),

Stage 2: core bonding and spacer plies (400 g/m^2 adhesive film). Cure at 100°C for 4 h, minimum 85% vacuum pressure (650 mmHg),

Stage 3: partial cure of a stabilizing adhesive layer to the core (250 g/m^2 adhesive film). Cure at 100°C for 2 h, minimum 85% vacuum pressure (650 mmHg),

Stage 4: backing skin and edge pan plies (250 g/m^2 adhesive film). Cure at 100°C for 4 h minimum 85% vacuum pressure (650 mmHg).

Following the manufacture of the test panels, the quality in terms of bond integrity and consolidation, was assessed using ultrasonic non-destructive testing.

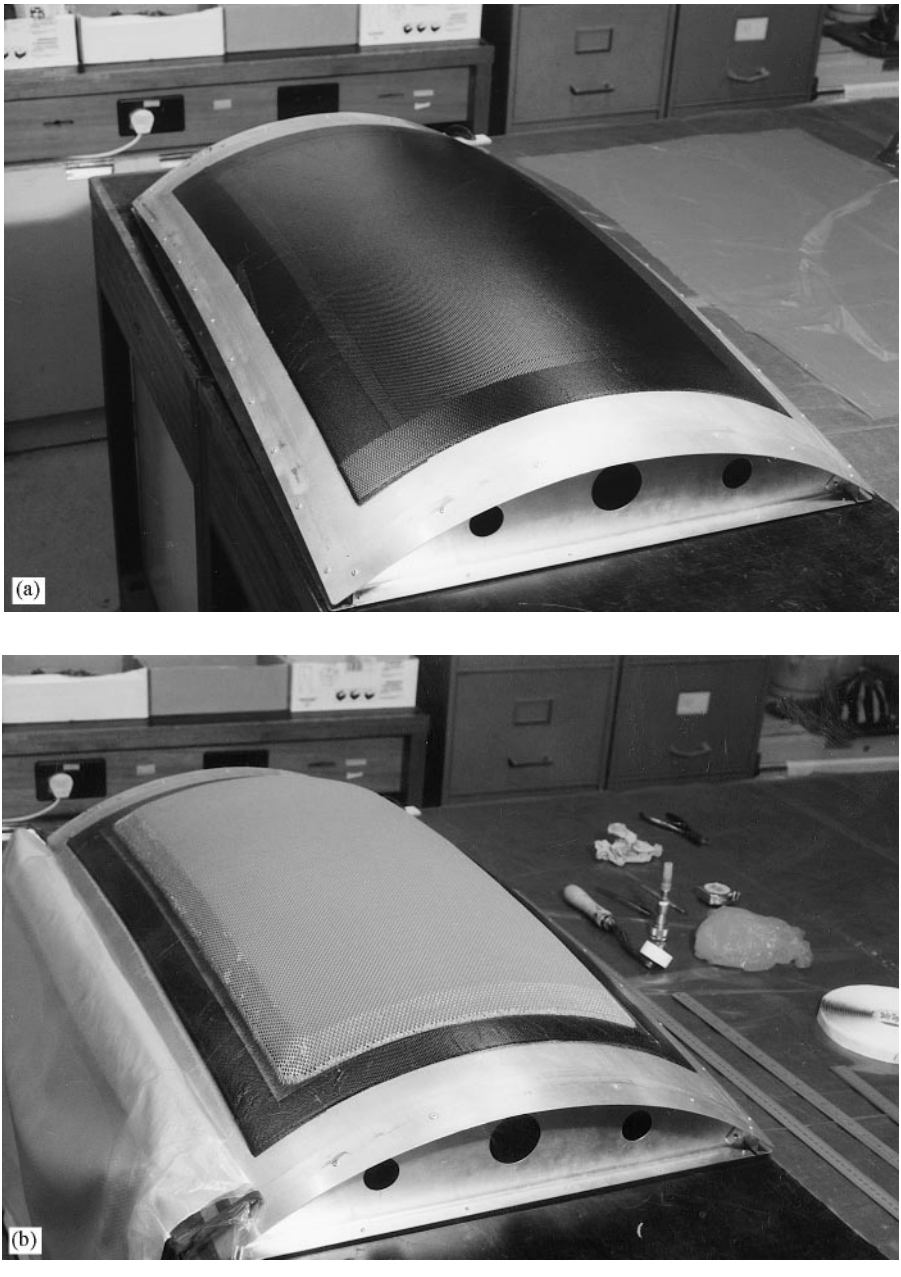

Figure 3. Doubly curved CFRP/honeycomb sandwich panel manufacturing process: (a) Stage 1—facing skin and doubler plies; (b) Stage 2—first adhesive film layer, core and spacer plies; (c) Stage 3—second adhesive film layer (partial cure); (d) Stage 4—third adhesive film layer, backing skin and edge pan plies; (e) Finished panel (prior to being trimmed to size).

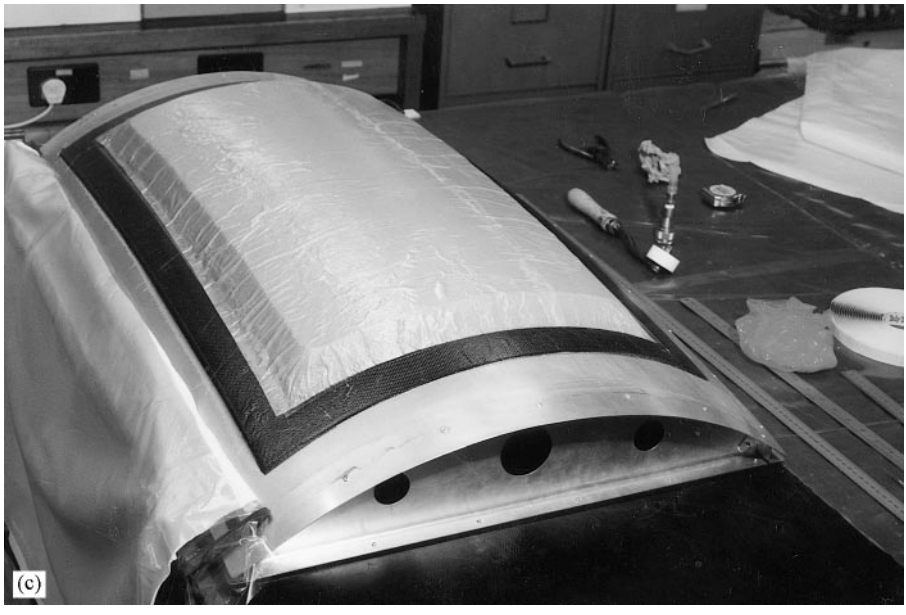

Figure 3. Continued.

This was carried out by hand using an A-Scan machine. All of the panels were found to be satisfactory with a good bond and consolidation.

3. EXPERIMENTAL PROCEDURE

3.1. CALIBRATION OF THE VIBRATION TEST EQUIPMENT

The vibration test equipment, which consisted of an ENDEVCO® impact hammer incorporating an ISOTRON® force sensor with a plastic tip and an

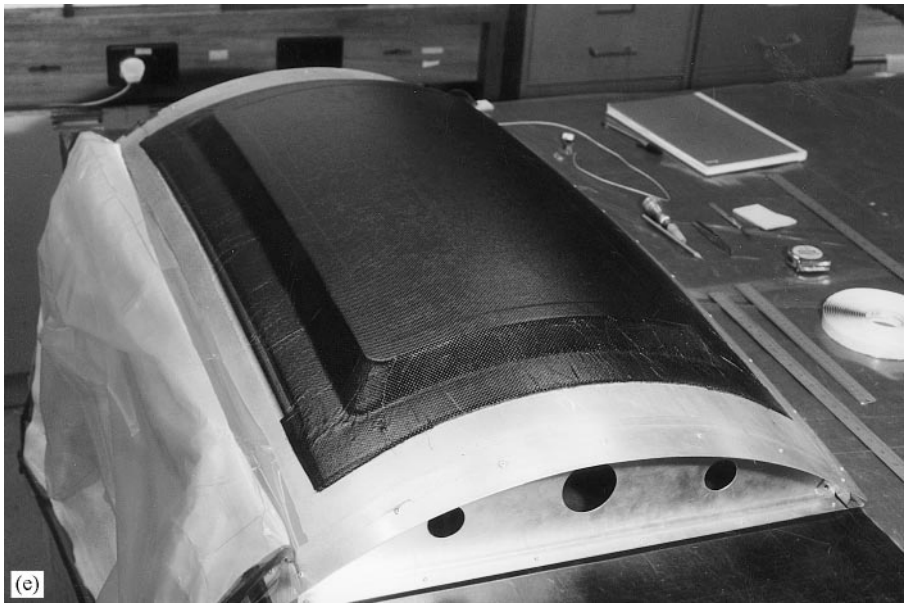

Figure 3. Continued.

TABLE 1

Ply lay-up details for the experimental test panels

Layer	Number of plies	Ply orientation
Facing skin	4	$[0/45]_s$
Doublers	2	[0/30]
Spacers	2	$[0_2]$
Edge pan	3	[0/45/0]
Backing skin	4	$[0/45]_s$

ENDEVCO® Model 2256A piezoelectric accelerometer, was calibrated using a known rigid mass suspended on two light wires. The accelerometer was secured to one end of the block using beeswax, and the other end was tapped 10 times using the impact hammer. The resulting signals were captured using a NATIONAL INSTRUMENTS VXI™ A/D converter and the accelerence FRF was obtained and averaged over the 10 measurements. The overall sensitivity was found to be $0{\cdot}453\,(\mathrm{V\,N})\cdot(\mathrm{V\,m/s^2})^{-1}$, and the ratio of the manufacturer's quoted sensitivities of the accelerometer and hammer was

$$\frac{10{\cdot}112\times10^{-3}}{22{\cdot}7\times10^{-3}}\left[\frac{\mathrm{V\,(m/s^2)^{-1}}}{\mathrm{V/N}}\right]=0{\cdot}445\left[\frac{(\mathrm{V\,N})}{(\mathrm{V\,m/s^2})}\right]$$

giving a 1·8% difference.

3.2. VIBRATION TESTING

Each panel was freely supported using bungee cords attached to a stiff frame. A grid of 40 measurement points was marked on each panel in order to recover the mode shapes from the test results. During the experiments, the hammer auto-power force spectrum was checked prior to saving the data to ensure a smooth spectrum with a reasonable input energy up to around 400 Hz. The cleanest hammer signal with a reasonably flat spectrum up to 400 Hz was produced by exciting the panels on the flange region, rather than in the main body of the panel. It was for this reason that the accelerometer was moved from point to point and the excitation position remained fixed. Five measurements were recorded per position and the hammer and accelerometer signals were recorded simultaneously, after passing through a low pass filter with a cut-off frequency of 1 kHz, using a VXI™ A/D converter. A sampling rate of 8000 Hz was used with a total number of 10 000 samples being recorded, giving 1·25 s of data. Since the acceleration time domain signal decayed significantly in the sample window (the decay in amplitude was of the order of 50–60 dB) any possible errors which could be introduced by leakage were considered negligible. Therefore, a rectangular window was used over the entire 10 000 samples (force and acceleration) giving a frequency resolution of 0·8 Hz and the digitized time histories were transformed to the frequency domain using the MATLAB™ "spectrum" function [13] which uses a radix-2 FFT algorithm. The accelerance frequency response function was obtained and averaged over the five measurements.

3.3. EXPERIMENTAL RESULTS

Typical plots of the real and imaginary parts of the accelerance for all three panels are shown in Figure 4 for panels 1, 2, and 3. The real and imaginary parts are shown to clearly indicate a resonance which is characterized by the real part crossing the zero axis accompanied by a sharp peak in the imaginary part at this point of crossing. As can be seen, the peaks are very sharp indicating a very low level of damping present. The damping ratio was found using the half-power point method and the linear magnitude of accelerance,

$$\zeta = \frac{(\omega_2 - \omega_1)}{2\omega_n}, \tag{1}$$

where ω_n is the frequency which corresponds to the resonance peak amplitude A_{max} and ω_1 and ω_2 are the frequencies either side of ω_n which correspond to $A_{max}/\sqrt{2}$. The damping ratio was found to be approximately 0·003 for each of the first three modes and for all three panels. The results also show well-spaced resonance frequencies for the first three modes. This allowed the resonant response of each of the first three modes to be treated as a single-degree-of-freedom response, hence estimates of the mode shapes were obtained from the imaginary part of the accelerance. The first three experimental mode shapes for panel number one are shown in Figure 5. The mode shapes for panel numbers two and three were found to be very similar.

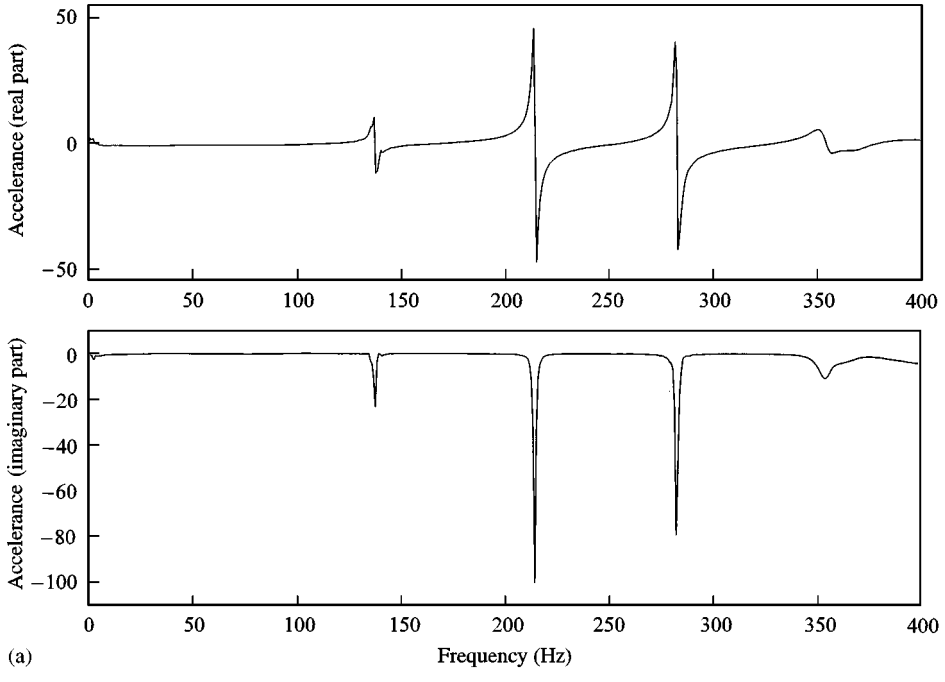

(a)

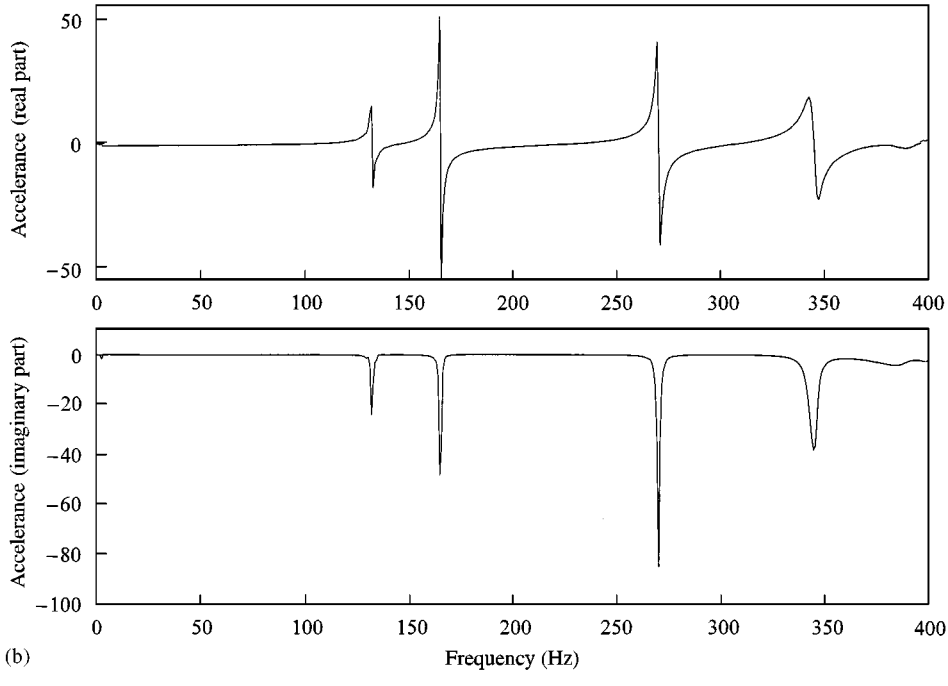

(b)

Figure 4. Real and imaginary parts of the accelerance for the three experimental test panels. Freely supported. Excitation point and measurement locations given in arc lengths (x = long side, y = short side) from the bottom left hand corner of the panel on the inside (concave) face: (a) panel #1 (Excitation point: $x = 360$ mm, $y = 48$ mm; Accelerometer position: $x = 307$ mm, $y = 90$ mm); (b) panel #2. (Excitation point: $x = 360$ mm, $y = 48$ mm. Accelerometer position: $x = 309$ mm, $y = 85$ mm; (c) panel #3. (Excitation point: $x = 360$ mm, $y = 48$ mm. Accelerometer position: $x = 202$ mm, $y = 464$ mm).

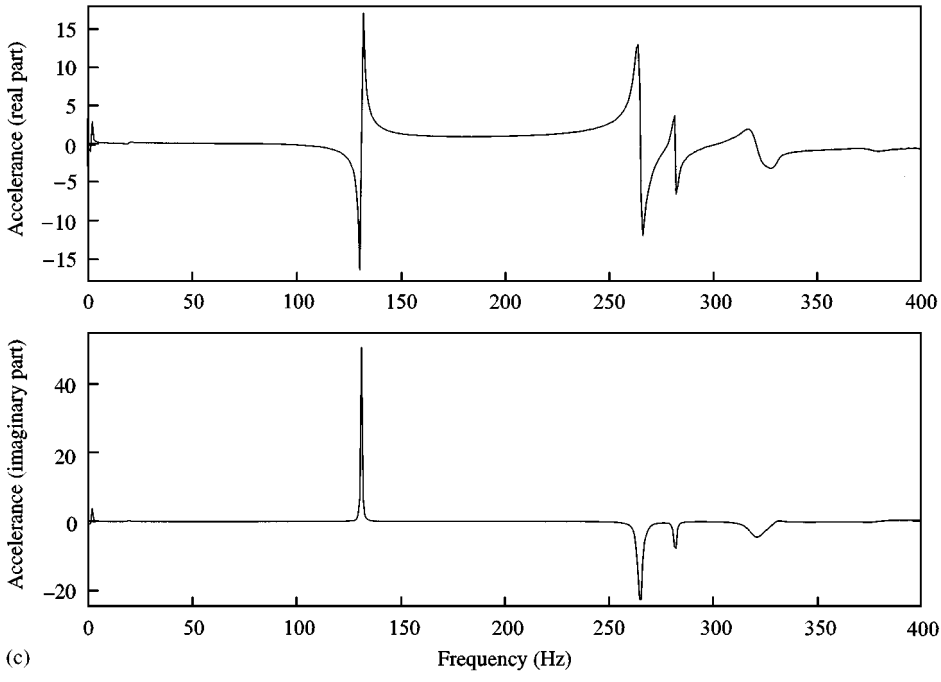

Figure 4. Continued.

4. FINITE ELEMENT ANALYSIS

4.1. DEVELOPMENT OF THE MODEL

The ANSYS™ [14] finite element package was used to analyze the doubly curved panels. Due to the geometry of the panels and the complex lay-up details, particularly around the bevelled edge, the model was built by constructing the doubly curved surface in the global Cartesian co-ordinate system and meshing this with SHELL91™ elements. This is a layered element which offers the choice of a "sandwich option", whereby the middle layer is assumed to be thick (greater than $\frac{5}{7}$ of the total thickness) and orthotropic, and is assumed to carry all of the transverse shear. The SHELL91™ element has eight nodes with six degrees of freedom per node with the option of nodal location at the top, middle or bottom surface. The complex bevelled edge region was initially modelled by modifying the real constants (specifically the lay-up details) for the elements [15], and the nodes were located along the bottom surface ($z = 0$) of each element to ensure that the flange and associated constraint nodes were located in the correct position, as shown in Figure 6. The detail of the chamfer was not initially included since the influence of this detail on the natural frequencies of vibration for a panel having freely supported boundary conditions was deemed to be small. However, for any other boundary condition (simply supported or fully clamped), this chamfered region could have a profound effect [16], particularly in terms of the panel edge strains for a forced response analysis. The model was therefore made more representative by introducing the chamfer which was achieved by altering the

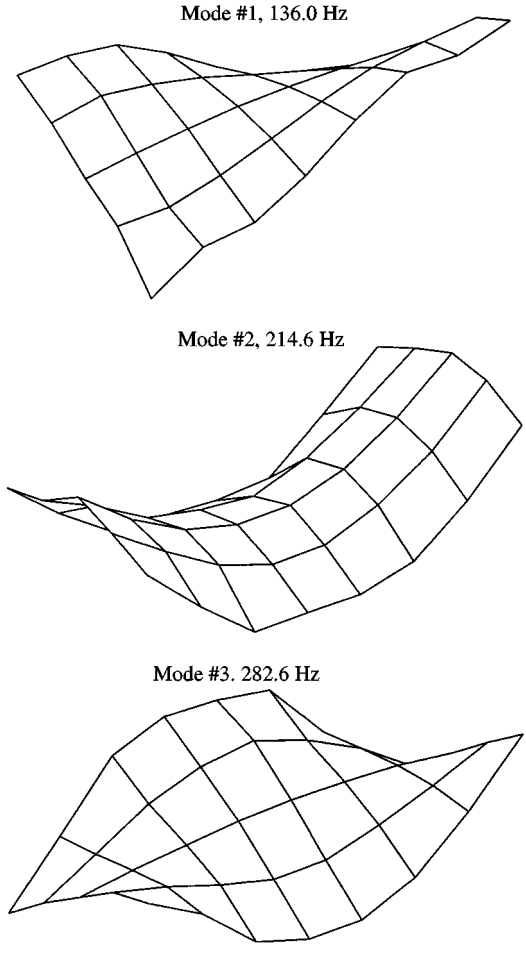

Figure 5. The first three mode shapes for panel #1 (measured).

element thickness real constants for the elements in this region. Both the initial and chamfered edge models, and the chamfer detail, are shown in Figure 6 where the models have been plotted in terms of their real constant (thickness) values. The material properties used in the models are given in Table 2.

4.2. FE RESULTS

Both models were analyzed with freely supported boundary conditions, using a networked Sun machine which was one of eight 60 MHz processors (each with floating point unit) controlled by a SunSPARC Server 1000. The predicted natural frequencies for the first four non-rigid body modes are shown in Table 3 for both the initial and chamfered edge models and for all three panel geometries. These results are compared with resonance frequencies obtained from the experiments and the percentage difference is indicated, although the difference values do not take into account uncertainties in the experiment and FE analysis. The results

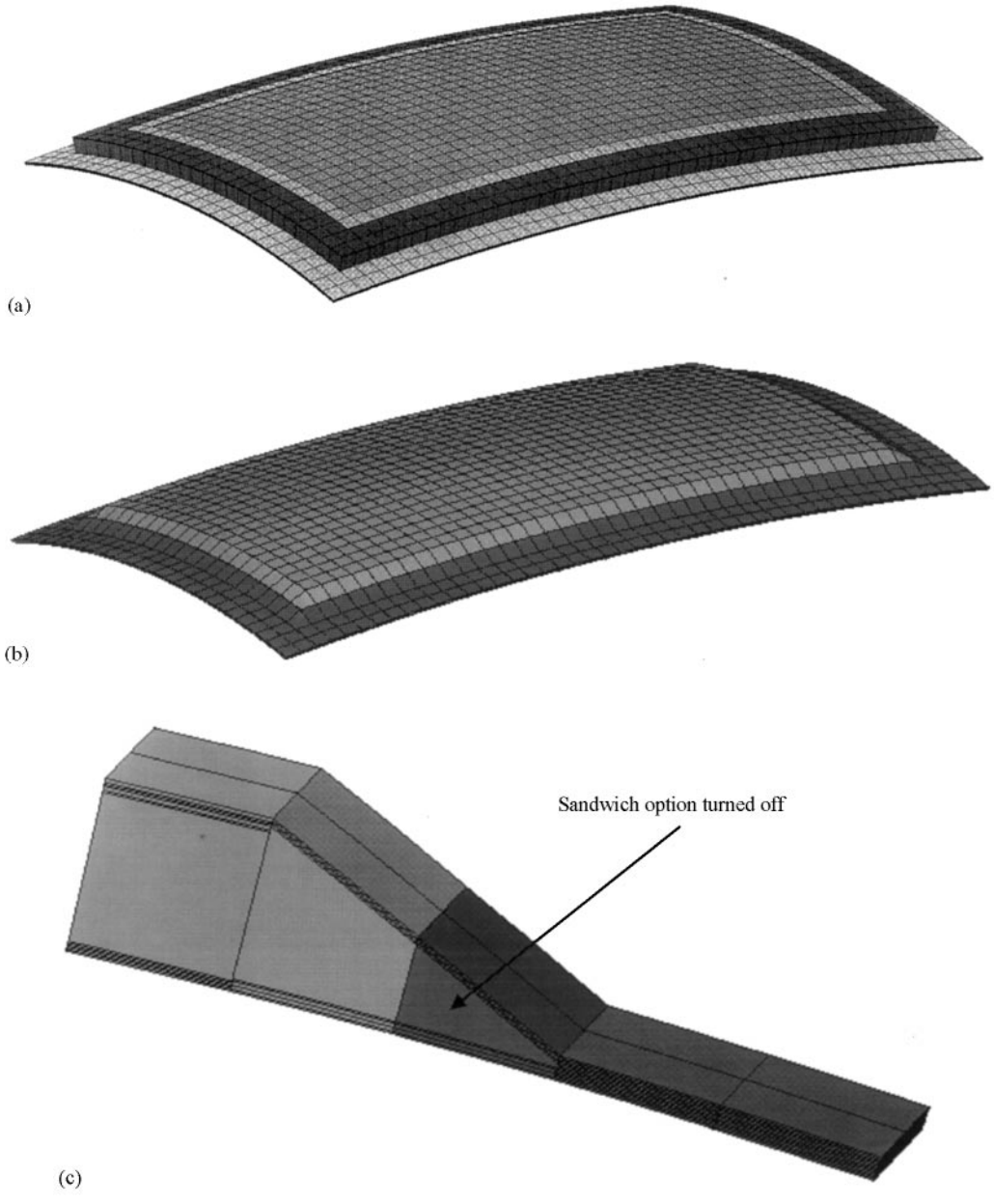

Figure 6. Development of the finite element model: (a) initial model (panel # 1); (b) chamfered edge model (panel # 1); (c) detail of the chamfer region.

obtained do, however, show excellent agreement when compared with the experimental results for the lower natural frequencies of vibration. All of the models had approximately 23 000 active degrees of freedom (d.o.f.'s) with $\sim$ 1200 elements, and the CPU time to obtain the first four non-rigid body modes was $\sim$ 1080 s (total elapsed time $\sim$ 2100 s). In order to check the convergence of the results,

TABLE 2

Material specifications for the experimental test panels

Layer	Thickness	Elastic modulus (Pa)		Shear modulus (Pa)				Density (kg/m^3)	Poisson's ratio
	(m)	E_{11}	E_{22}	E_{33}	G_{12}	G_{xz}	G_{yz}		
CFRP†	0·25e-3	57·93e9	57·93e9	—	3·7e9	—	—	1518·0	0·04
Honeycomb	19·0e-3	0	0	120e6	0	35e6	20e6	48·0	—

† Properties obtained using cured test specimens with $[0_4]$ and $[45_4]$ ply lay-up and with 60% fibre volume fraction.

TABLE 3

Comparison of measured and predicted resonance/natural frequencies of the three freely supported test panels

Measured (Hz)	ANSYS results (Initial model) (Hz)	Difference (%)	ANSYS results (Chamfered edge model) (Hz)	Difference (%)
		Panel #1		
136·0	134·4	− 1·2	139·3	− 2·4
214·6	217·4	1·3	221·7	− 3·2
282·6	275·8	− 2·4	284·5	− 0·67
352·1	367·2	4·3	370·8	− 5·04
		Panel #2		
131·5	130·5	− 0·75	134·2	− 2·0
164·7	166·0	0·75	169·3	− 2·7
269·0	260·2	− 3·3	270·2	− 0·44
343·1	347·8	1·4	349·7	− 1·9
		Panel #3		
130·9	127·9	2·3	132·7	− 1·4
264·5	278·1	− 4·9	279·7	− 5·4
280·9	294·0	− 4·4	302·8	− 7·2
320·4	340·7	− 5·9	345·0	− 7·1

a finer mesh was used giving 90 000–93 000 active d.o.f.'s ($\sim$ 5000 elements). This resulted in a change in the predicted natural frequencies of $\approx 0{\cdot}7\%$ compared with the coarser mesh model. The processing time, however, was significantly increased (CPU time $\sim$ 14 600 s, total elapsed time $\sim$ 17 700 s) and it was highly probable that the limits of the solver were being reached with so many active d.o.f.'s. Therefore, the models with approximately 23 000 active d.o.f.'s were considered accurate enough for use in further investigations. Comparison is also made between the initial and chamfered edge model. The main drawback with the chamfered edge model is that when using SHELL91™ elements, the "sandwich option" cannot be used where the core is less than $\frac{5}{7}$ of the total thickness. Therefore, the "sandwich option" had to be turned off in part of the chamfered region, as shown in Figure 6(c). This had the effect of introducing extra stiffness into the model since the middle core layer of the elements in this region cannot carry all of the transverse shear. This effect is seen in Table 3 where the predicted natural frequencies are slightly higher than those obtained using the initial model. The main drawback with the initial model is the discontinuity introduced in the layup around the bevelled edge region. Although not necessarily a problem in terms of predicting natural frequencies of vibration for panels with freely supported boundary conditions, the model would produce a discontinuous strain distribution around the bevelled edge region for any other boundary condition when conducting a forced response analysis. It can be said, therefore, that the chamfered edge FE

model can be used with confidence for predicting the natural frequencies of vibration of the doubly curved sandwich panels, which is reinforced when one compares the first three mode shapes obtained from the FE analysis with those obtained experimentally, as shown in Figures 7 and 5 respectively. The chamfered

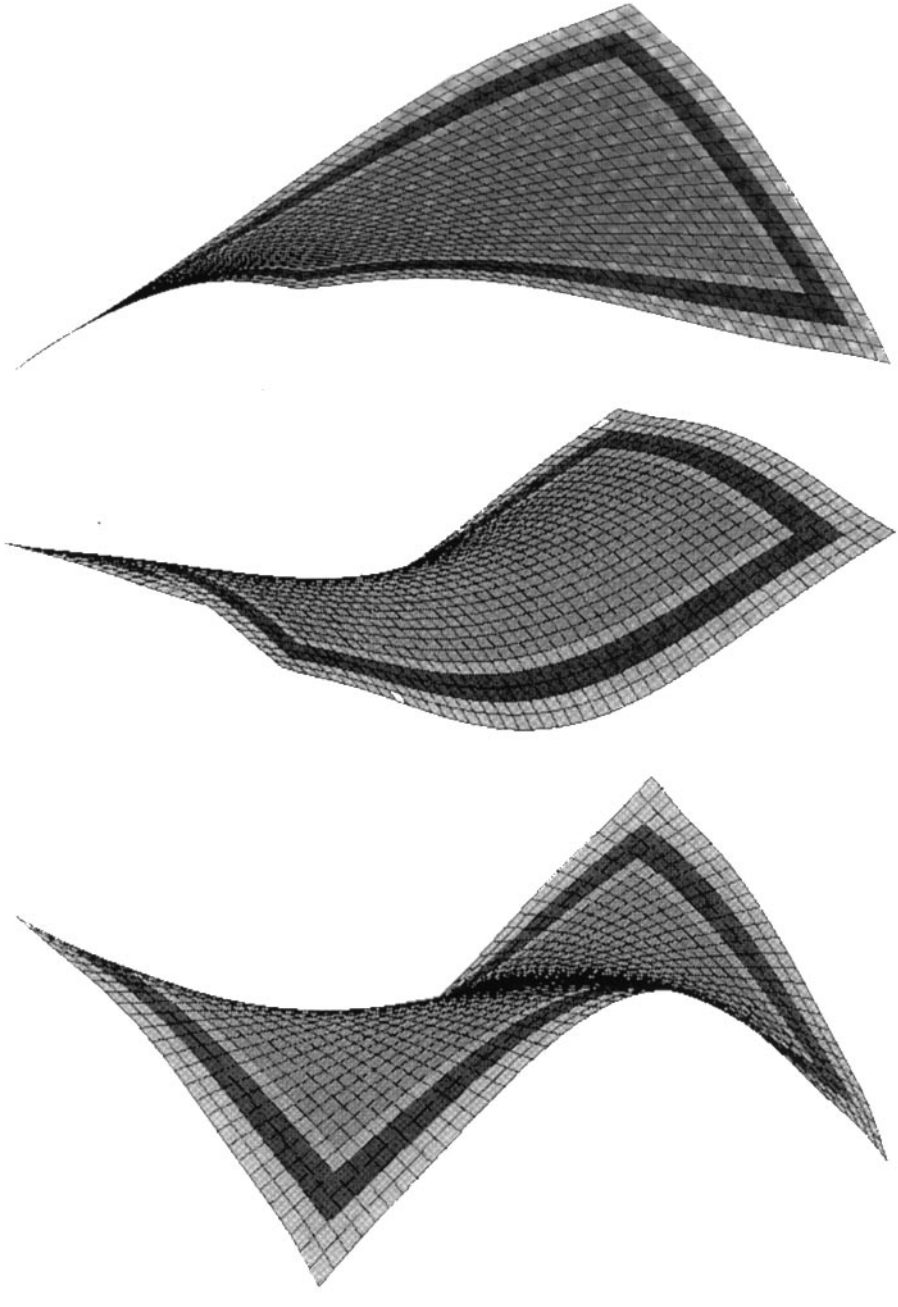

Figure 7. The first three mode shapes (FE).

edge FE model will be validated further by comparing strains obtained from PWT tests at a later stage in the study.

5. PARAMETER STUDIES USING THE FE MODEL

The chamfered edge FE model was used to investigate the effects of various design parameters on the natural frequencies of vibration of doubly curved rectangular sandwich panels with various boundary conditions. In all cases, the surface area of the panels was kept constant along with the number of plies, ply thicknesses, Young's modulii, and the ply and core densities.

5.1. THE EFFECT OF RADII OF CURVATURE ON THE FIRST FOUR NATURAL FREQUENCIES OF VIBRATION

The effect of changing radii of curvature on the natural frequencies of vibration was investigated for a panel having the dimensions $a = 0{\cdot}915$ m $\times\, b = 0{\cdot}531$ m, material properties as shown in Table 2, and lay-up as shown in Table 1. Three boundary conditions were considered; freely supported, fully clamped along all four edges, and "pinned" whereby the translational degrees of freedom were constrained along all four edges (the nodes were aligned with the global Cartesian co-ordinate system, hence in plane motion was not constrained in this case). Four long-side radii cases, $R_x = 0{\cdot}5$, 1·0, 2·0 and 10·0 m were considered, and the short-side radius was varied between 0·4 and 4 m for each of these four cases.

The results for the freely supported boundary condition are shown in Figure 8. For all of the long-side radii cases considered here the fundamental natural frequency is relatively invariant with changes in the short-side radius of curvature, which is understandable since the surface area has been kept constant and this frequency corresponds with the first torsional mode of vibration, as indicated in the figure. A slight decrease in the fundamental frequency is observed for short-side radii smaller than 0·8 m for all four long-side radii cases, whereas the second and third natural frequencies exhibit an increase in frequency with decreasing short-side radius. The second natural frequency is associated with the first bending mode of vibration, and the effect of decreasing the short-side radius of curvature results in a rapid increase in the frequency of vibration which is more apparent for $R_x = 10{\cdot}0$ m, a case which tends towards that of a singly curved panel. In fact, as the panels become more doubly curved, the effect of changing the radii of curvature appears less pronounced for the freely supported boundary condition. For the case of $R_x = 0{\cdot}5$ m, the fundamental frequency corresponds with the first bending mode of vibration for short-side radii down to $R_x = 1{\cdot}2$ m, at which point the curves for the first and second natural frequency appear to almost touch and after which the torsional and bending modes appear to interchange as the curves veer away from each other. This phenomenon, known as "curve veering", has been well reported by many authors [17–21], and can be clearly seen for the "pinned" and fully clamped cases, as shown in Figures 9 and 10 respectively. Here, reducing the short-side radius of curvature has the effect of increasing the natural frequencies of vibration,

although it is interesting to note that for $R_x = 2{\cdot}0$ and $10{\cdot}0$ m, and for both boundary conditions, the frequency of vibration of the (1, 2) mode seems to be relatively invarient with decreasing R_y down to $1{\cdot}2$ m, after which it increases. For the case of $R_x = 0{\cdot}5$ m and for both "pinned" and fully clamped boundary

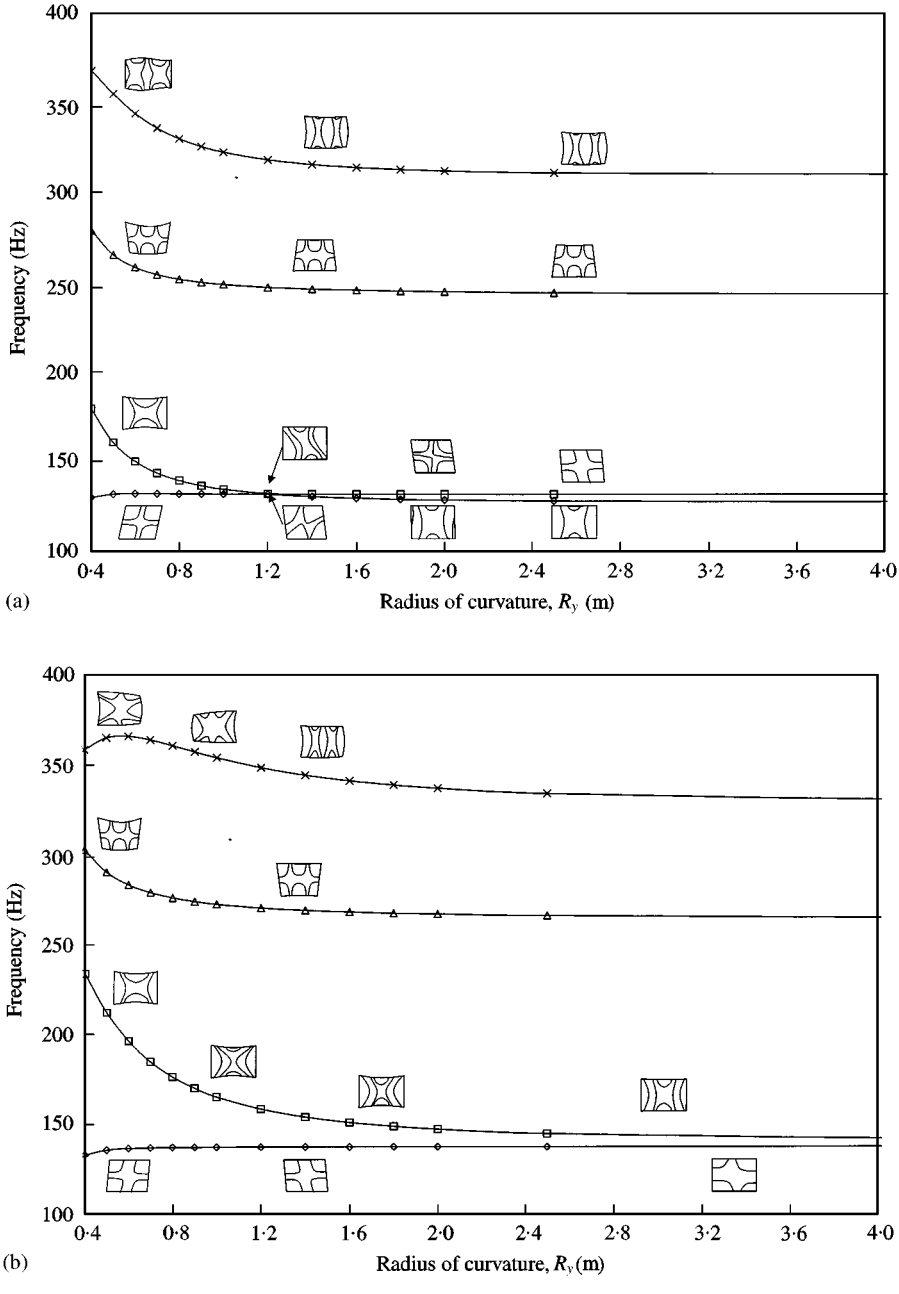

Figure 8. Effect of changing radius of curvature (R_y—short side) on the first four (non-rigid body) natural frequencies. Freely supported. (Key to natural frequency number: ◇: I, □, II, △: III, ×: IV): (a) $R_x = 0{\cdot}5$ m; (b) $R_x = 1{\cdot}0$ m; (c) $R_x = 2{\cdot}0$ m; (d) $R_x = 10{\cdot}0$ m.

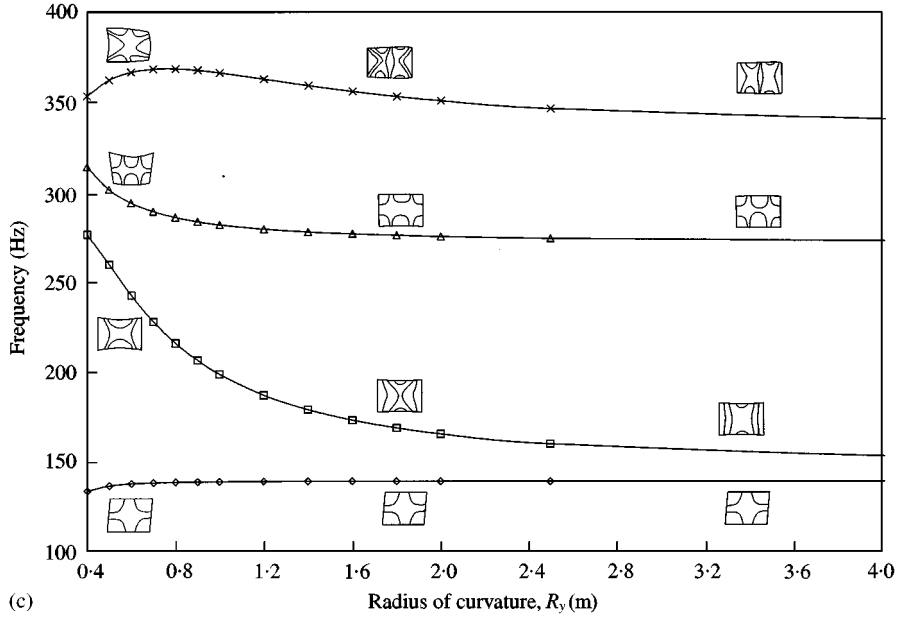

(c)

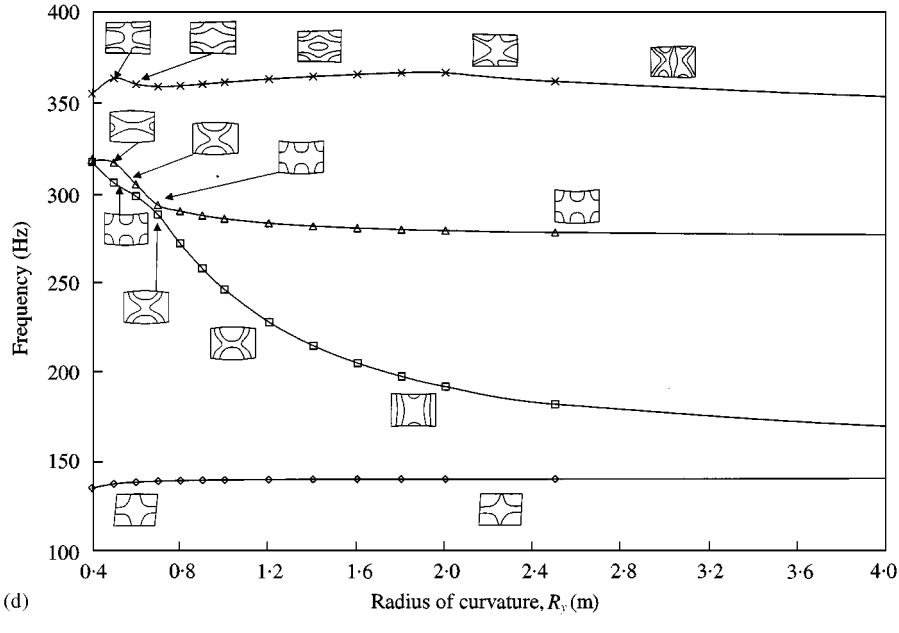

(d)

Figure 8. Continued.

conditions, the first four natural frequencies increase at approximately the same rate with very little interchange of the mode shapes occurring. At lower values of R_y, the fundamental frequency tends to decrease with reducing short-side radius of curvature, which does not occur for the other three long-side radius cases. In addition, the mode shapes becomes more complicated at lower values of R_y, especially for the $R_x = 0{\cdot}5$ m case.

5.2. THE EFFECT OF THE ORTHOTROPY OF THE CORE ON THE FIRST FOUR NATURAL FREQUENCIES OF VIBRATION

A sensitivity study was carried out to study the effect of changing the orthotropy of the core, which is represented by the ratio G_{xz}/G_{yz}, on the natural frequencies of

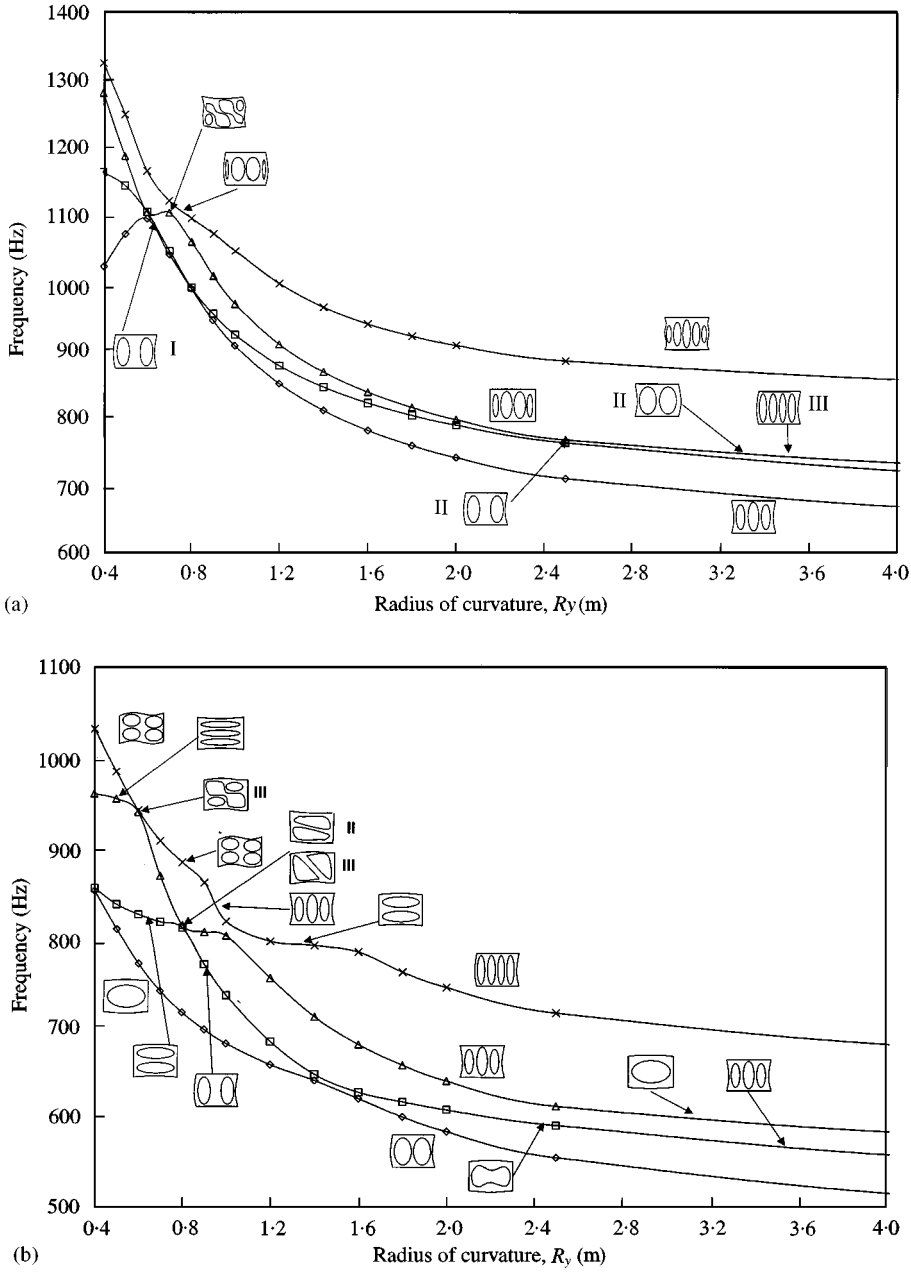

Figure 9. Effect of changing radius of curvature (R_y—short side) on the first four natural frequencies. Translational degrees of freedom constrained along all four edges. (Key to natural frequency number: ◇: I, □, II, △: III, ×: IV): (a) $R_x = 0{\cdot}5$ m; (b) $R_x = 1{\cdot}0$ m; (c) $R_x = 2{\cdot}0$ m; (d) $R_x = 10{\cdot}0$ m.

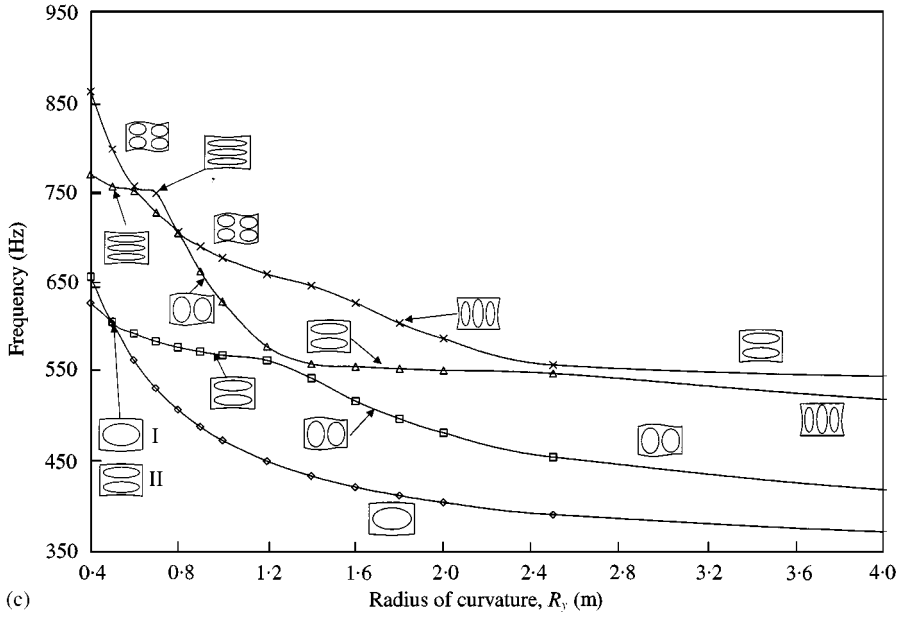

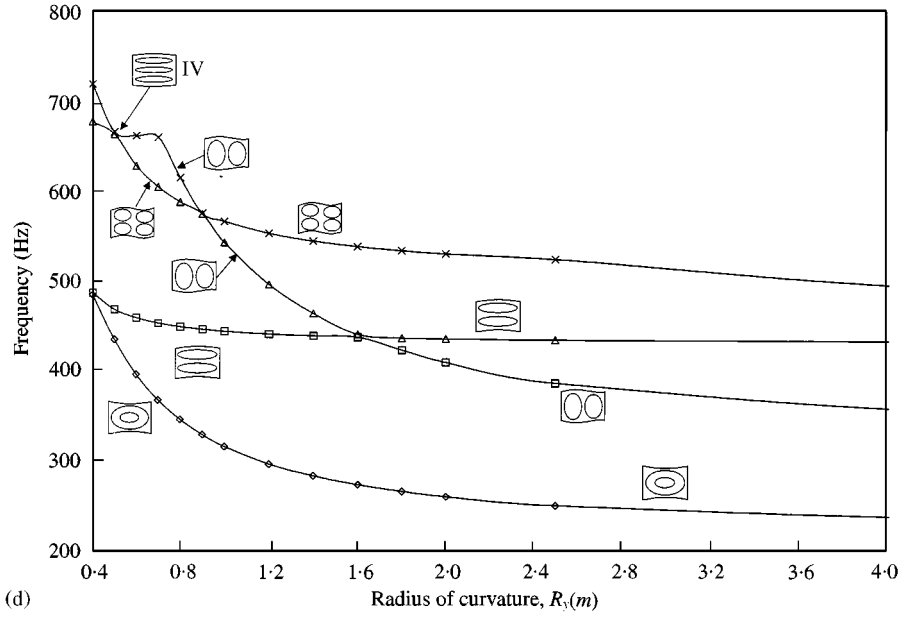

Figure 9. Continued.

vibration. The ratio was varied between 0·1713 and 1·256 (corresponding to -70 to $+120\%$ change about the original ratio of $G_{xz}/G_{yz} = \frac{20}{35} = 0{\cdot}571$) by keeping the value G_{xz} constant whilst varying G_{yz}. Both low and high shear stiffnesses were considered; $G_{xz} = 20$ MPa and G_{yz} varying between 15·92 and 116·75 MPa, and with both G_{xz} and G_{yz} reduced by an order of magnitude respectively. Three panel cases were investigated; $R_x = 3{\cdot}5\text{ m} \times R_y = 1{\cdot}0\text{ m}$, $R_x = 1{\cdot}2\text{ m} \times R_y = 1{\cdot}0\text{ m}$, and

$R_x = 3{\cdot}5\ \text{m} \times R_y = 0{\cdot}5\ \text{m}$ with the dimensions $a = 0{\cdot}915\ \text{m} \times b = 0.531\ \text{m}$ and with "pinned" and fully clamped boundary conditions. All other lay-up details and material properties were as detailed in Tables 1 and 2 respectively.

Figure 11 shows the results for the fully clamped boundary condition and for all three panel cases. The natural frequencies of vibration are seen to increase with

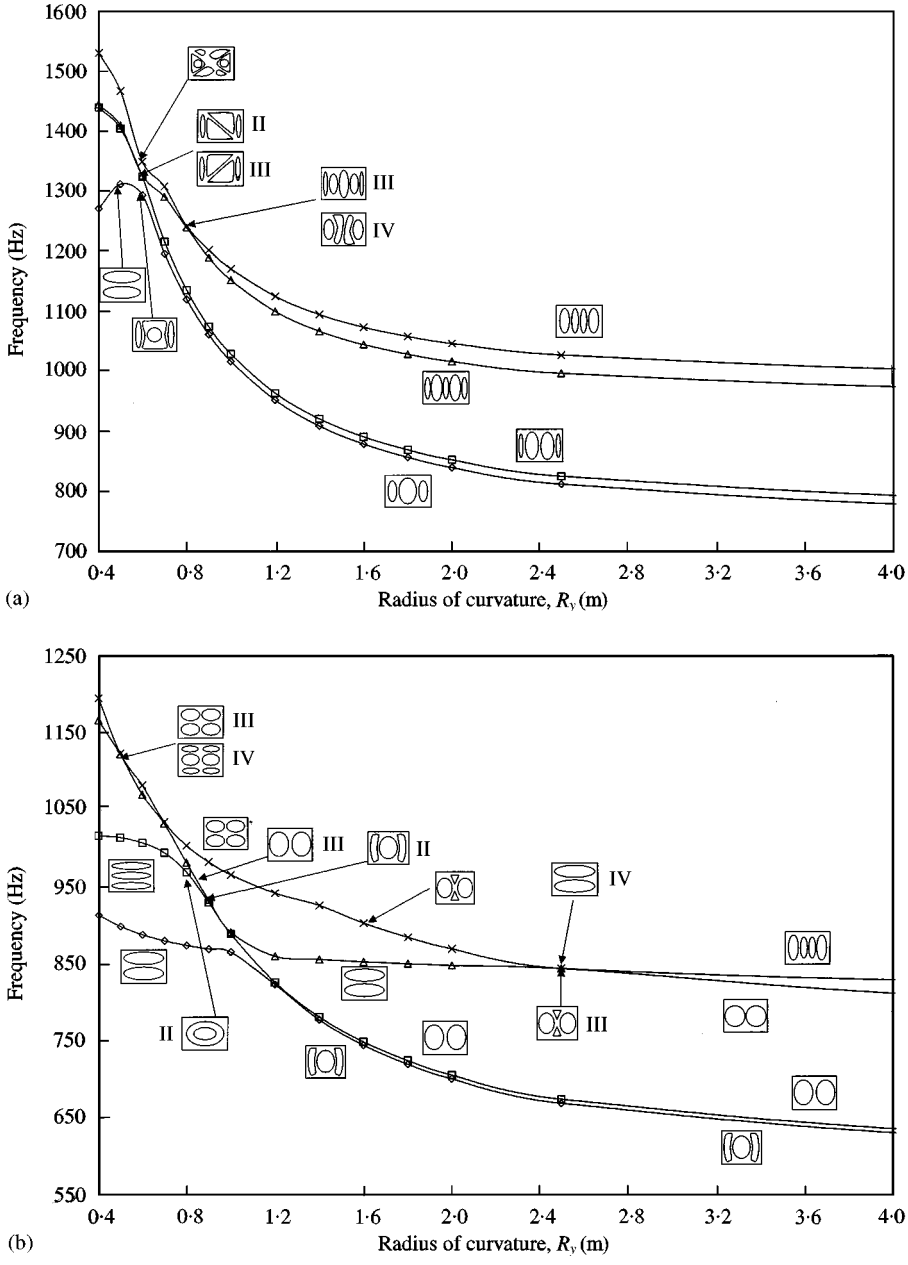

Figure 10. Effect of changing radius of curvature (R_y—short side) on the first four natural frequencies. Fully clamped along all four edges. (Key to natural frequency number: ◇: I, □, II, △: III, ×: IV): (a) $R_x = 0{\cdot}5$ m; (b) $R_x = 1{\cdot}0$ m; (c) $R_x = 2{\cdot}0$ m; (d) $R_x = 10{\cdot}0$ m.

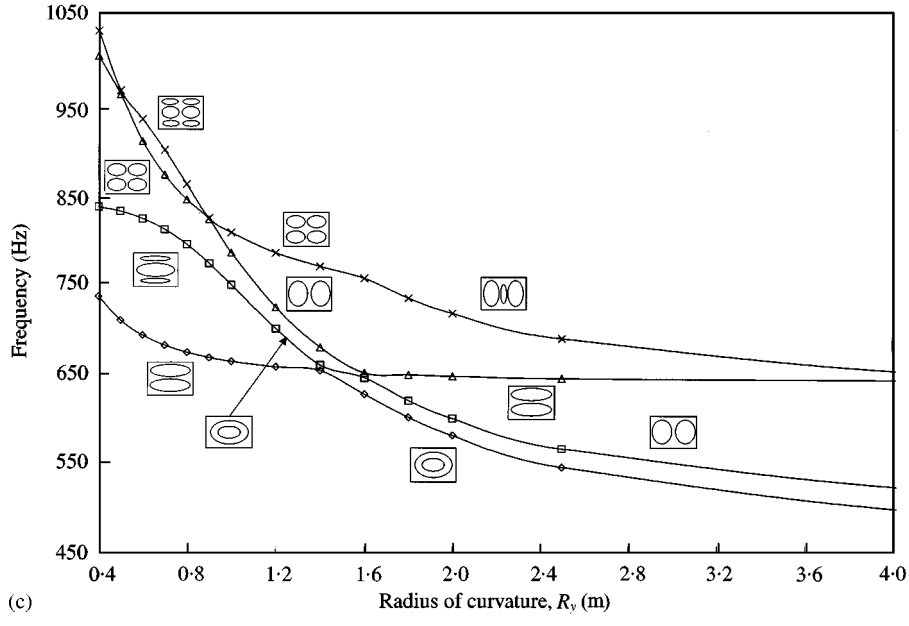

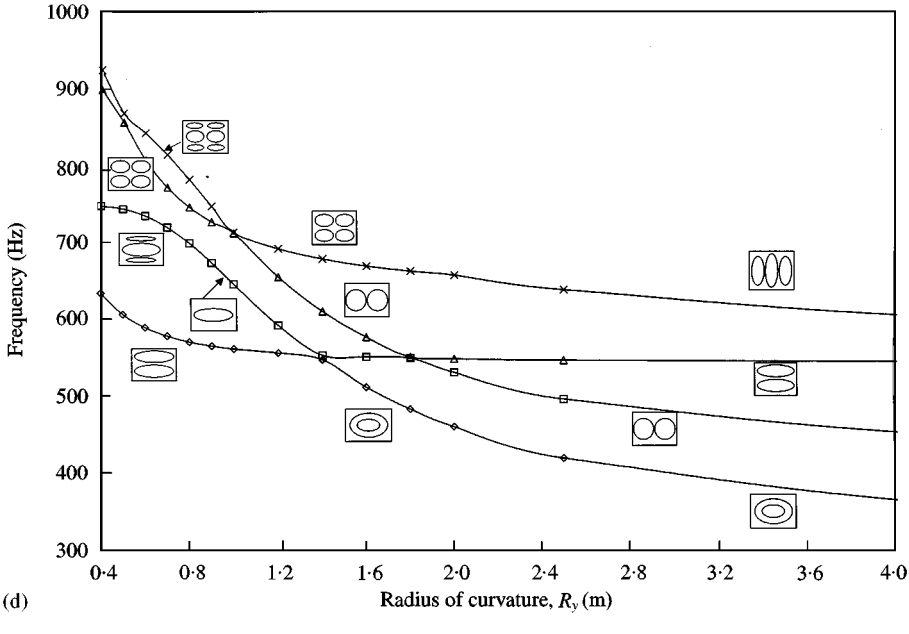

Figure 10. Continued.

decreasing orthotropy, i.e., as G_{yz} is increased. In all three cases, the rate of change of frequency with changing orthotropy is moderate, so from the point of view of sensitivity, small changes in the orthotropy about a certain value do not produce large changes in the frequencies of vibration. This rate of change is approximately the same for the high and low shear stiffness cases for orthotropic ratio values

above approximately 0·6. Below this, the lower shear stiffness core creates a sharper increase in frequency with decreasing orthotropy. Very little veering is observed with the fully clamped boundary condition, compared with the "pinned" boundary

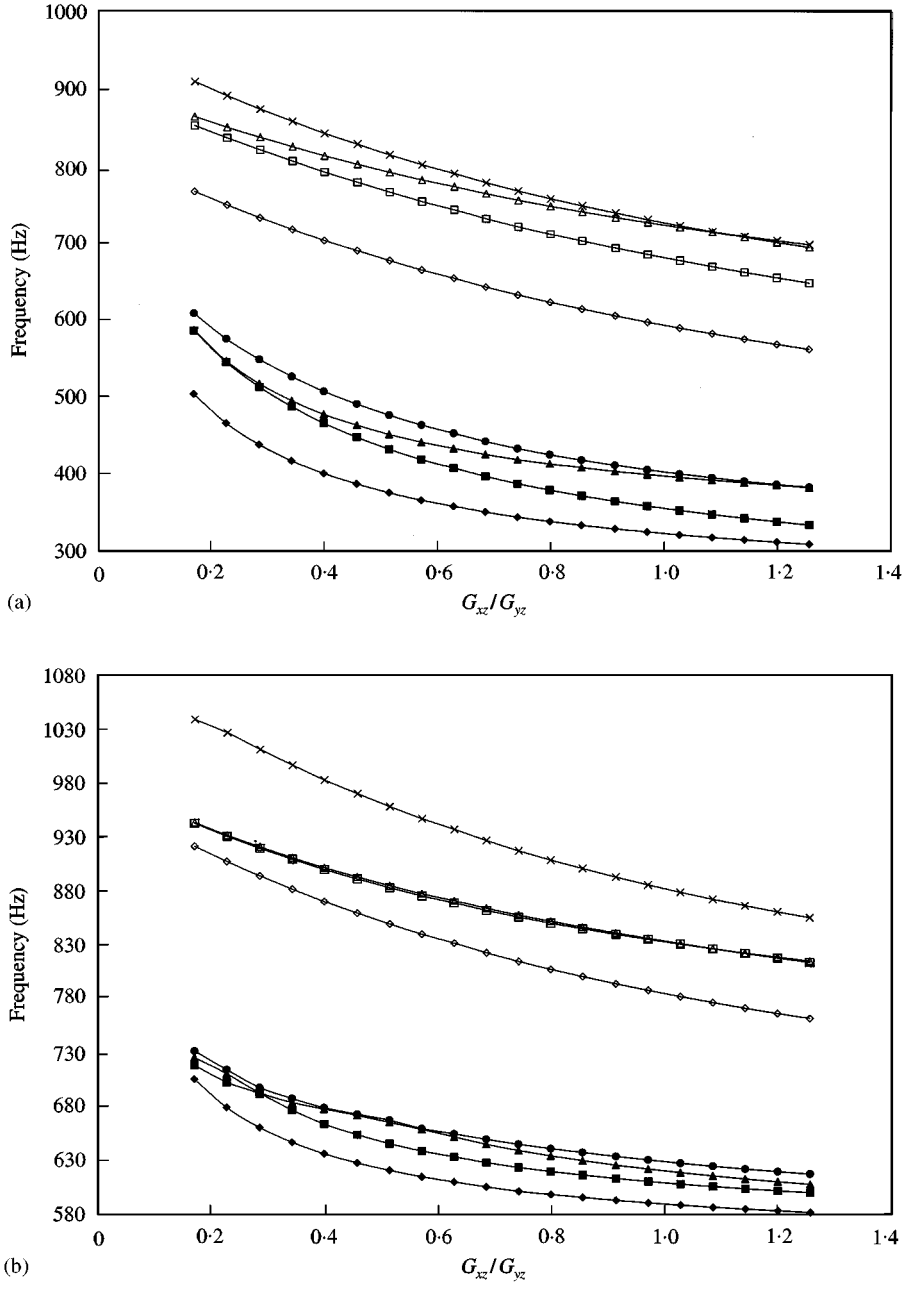

Figure 11. Effect of changing orthotropy on the first four natural frequencies. Fully clamped along all four edges. (Key to natural frequency number: High shear stiffness: ◇: I, □, II, △: III, ×: IV. Low shear stiffness ($G_{xz}/10$, $G_{yz}/10$): ◆: I, ■: II, ▲: III, ●: IV): (a) $R_x = 3{\cdot}5$ m, $R_y = 1{\cdot}0$ m; (b) $R_x = 1{\cdot}2$ m, $R_y = 1{\cdot}0$ m; (c) $R_x = 3{\cdot}5$ m, $R_y = 0{\cdot}5$ m.

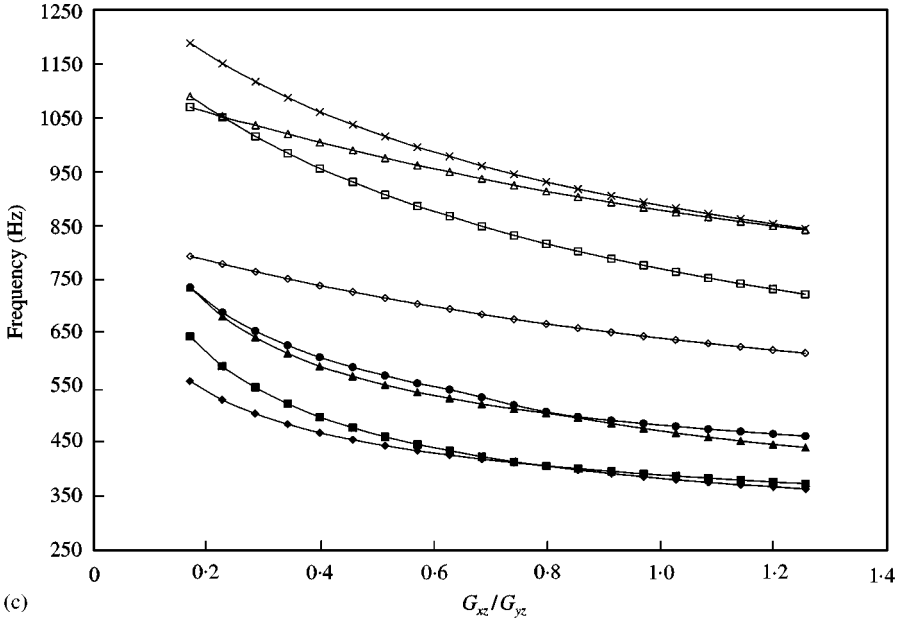

Figure 11. Continued.

condition which is shown in Figure 12. The veering phenomenon can be clearly seen in Figure 12(c) (inset), where a larger set of results have been obtained between $G_{xz}/G_{yz} = 0{\cdot}86$ and $G_{xz}/G_{yz} = 0{\cdot}9$ for the fourth and fifth natural frequencies of vibration. The effect of changing orthotropy appears to be less pronounced for the "pinned" case than for the fully clamped case, particularly for the fundamental natural frequency and for both high and low shear stiffness cores. In addition, the first four frequencies for the higher shear stiffness case are spread over a greater frequency band compared to the lower shear stiffness case, which can also be observed for the fully clamped boundary condition.

5.3. THE EFFECT OF PLY ORIENTATION ON THE FIRST FOUR NATURAL FREQUENCIES OF VIBRATION

The final parameter study was concerned with investigating the effect of changing ply orientation on the first four natural frequencies of vibration for the same three panel cases as those considered in this previous sub-section and for the "pinned" and fully clamped boundary conditions. The material properties used were those as given in Table 2, and the panel dimensions were again $a = 0{\cdot}915$ m $\times\, b = 0{\cdot}531$ m. Due to the large number of possible ply lay-ups, it was decided to investigate the change in orientation of the middle two layers of both the facing and backing skin, which were varied between 0 and 90° in 5° steps, whilst keeping the outer plies at 0°. The results for the "pinned" case are shown in Figure 13. As expected the results are symmetric about 45° due to the use of a balance plain weave material which has identical properties in the two orthogonal

directions E_x and E_y. The greatest change in frequency with ply orientation is for the $R_x = 1{\cdot}2$ m $\times R_y = 1{\cdot}0$ m case, where changes in mode shape are observed for the third and fourth natural frequencies of vibration, which could probably be

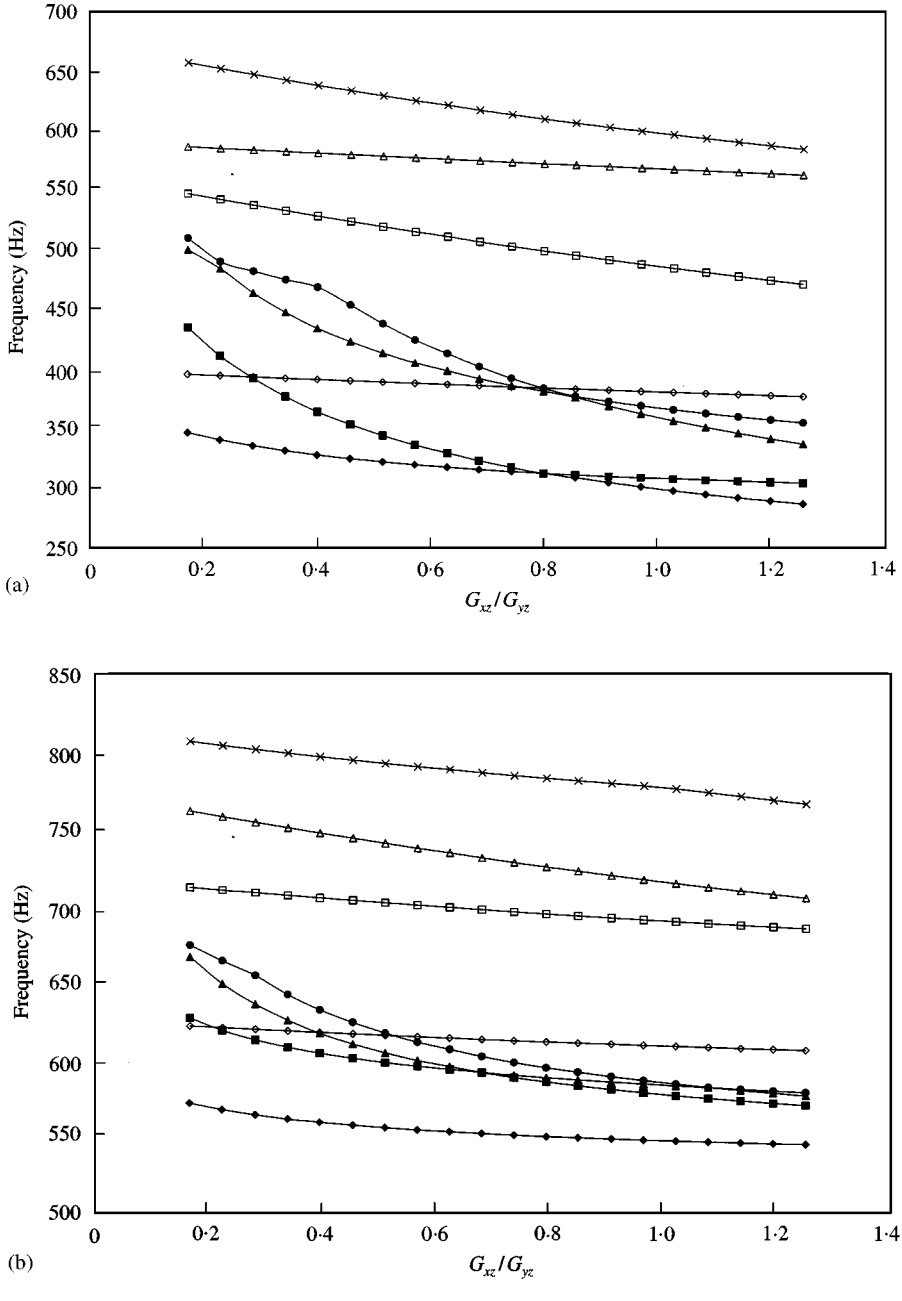

Figure 12. Effect of changing orthotropy on the first four natural frequencies. Translational degrees of freedom constrained along all four edges. (Key to natural frequency number: High shear stiffness: ◇: I, □, II, △: III, ×: IV). Low shear stiffness ($G_{xz}/10$, $G_{yz}/10$): ◆: I, ■: II, ▲: III, ●: IV: (a) $R_x = 3{\cdot}5$ m, $R_y = 1{\cdot}0$ m; (b) $R_x = 1{\cdot}2$ m, $R_y = 1{\cdot}0$ m; (c) $R_x = 3{\cdot}5$ m, $R_y = 0{\cdot}5$ m.

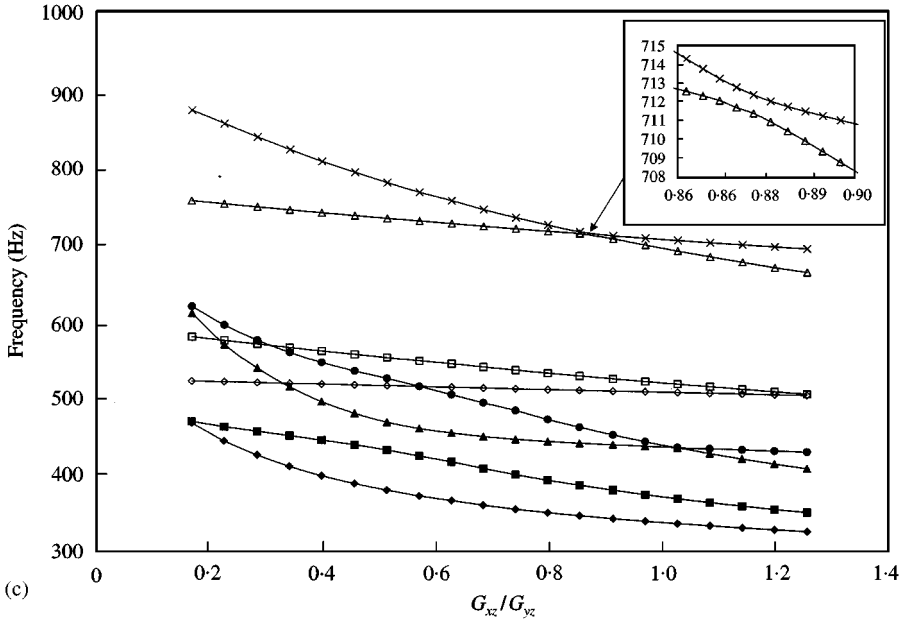

Figure 12. Continued.

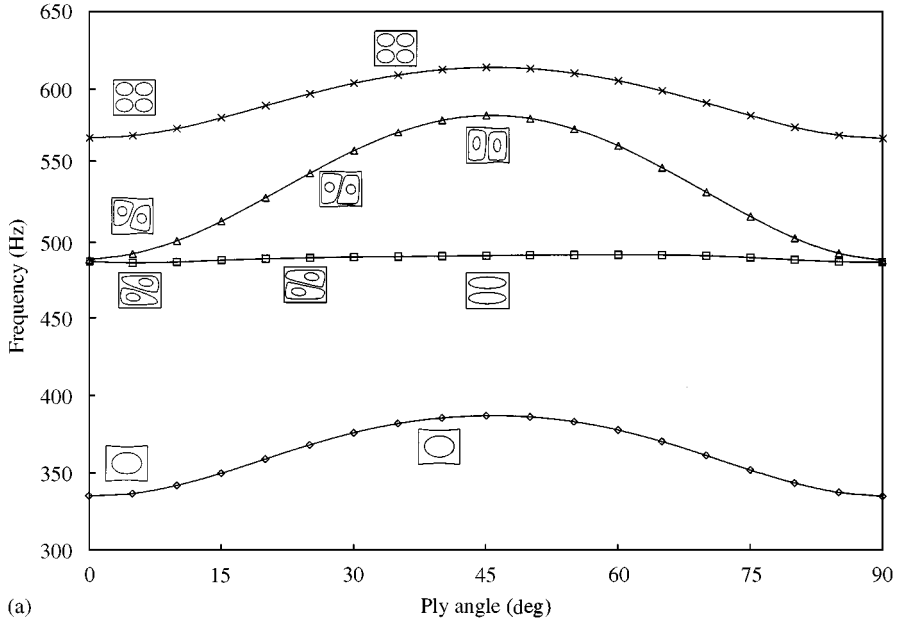

Figure 13. Effect of changing ply angle (middle two plies in the facing and backing skins) on the first four natural frequencies. Translational degrees of freedom constrained along all four edges. (Key to natural frequency number: ◇: I, □, II, △: III, ×: IV): (a) $R_x = 3{\cdot}5$ m, $R_y = 1{\cdot}0$ m; (b) $R_x = 1{\cdot}2$ m, $R_y = 1{\cdot}0$ m; (c) $R_x = 3{\cdot}5$ m, $R_y = 0{\cdot}5$ m.

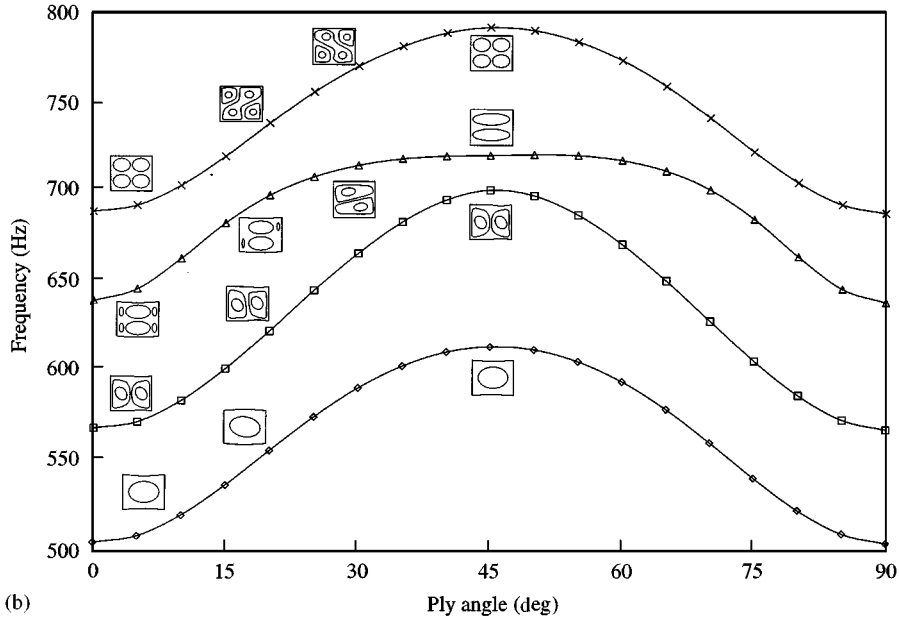

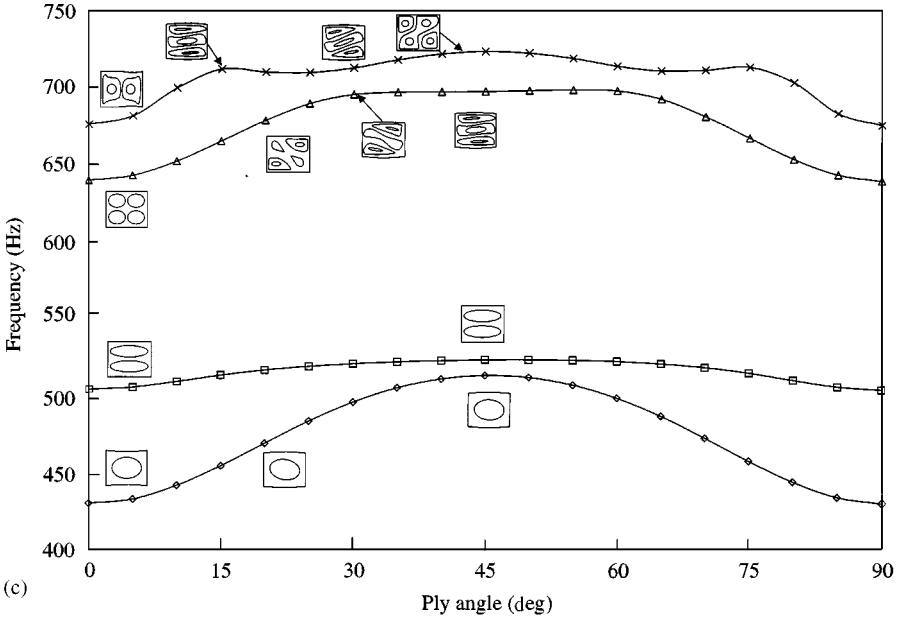

Figure 13. Continued.

ascribed to veering with a much higher frequency, or the well-known phenomenon of nodal lines aligning with the direction of dominant fibre reinforcement. In addition, it is interesting to note that the second natural frequency of vibration which again corresponds to the (1,2) mode, shows very little variation in frequency with the change in the parameter between 30 and 45°, particularly for the

$R_x = 3{\cdot}5\text{m} \times R_y = 1{\cdot}0$ m, case which shows little variation between 0 and 45°. Slight changes in the mode shape are observed with changes in the parameter, but no veering occurs, except for the fourth natural frequency of vibration for the $R_x = 3{\cdot}5$ m $\times R_y = 0{\cdot}5$ m case.

The results for the fully clamped boundary condition are shown in Figure 14. The results are again symmetric about the 45° ply orientation. The greatest change in frequency with variation in ply angle is observed for the $R_x = 3{\cdot}5$ m $\times R_y = 0{\cdot}5$m case, and the second natural frequency of vibration corresponding to the (1,3) mode is seen to show very little variation with changes in the parameter. Veering occurs more readily in all three cases, especially in the $R_x = 1{\cdot}2$ m $\times R_y = 1{\cdot}0$ m case, compared with Figure 13.

5.4. A SUMMARY OF THE MAJOR SENSITIVITIES

A relatively large amount of information has been presented concerning the effects of the various design parameters on the first four natural frequencies of vibration of doubly curved composite sandwich panels. Therefore, a brief summary of the major sensitivities is given below:

- For both the "pinned" and fully clamped boundary conditions, the panels with a long-side radius of $R_x = 0{\cdot}5$ m show the greatest overall change in frequency with variation in the short-side radius R_y.

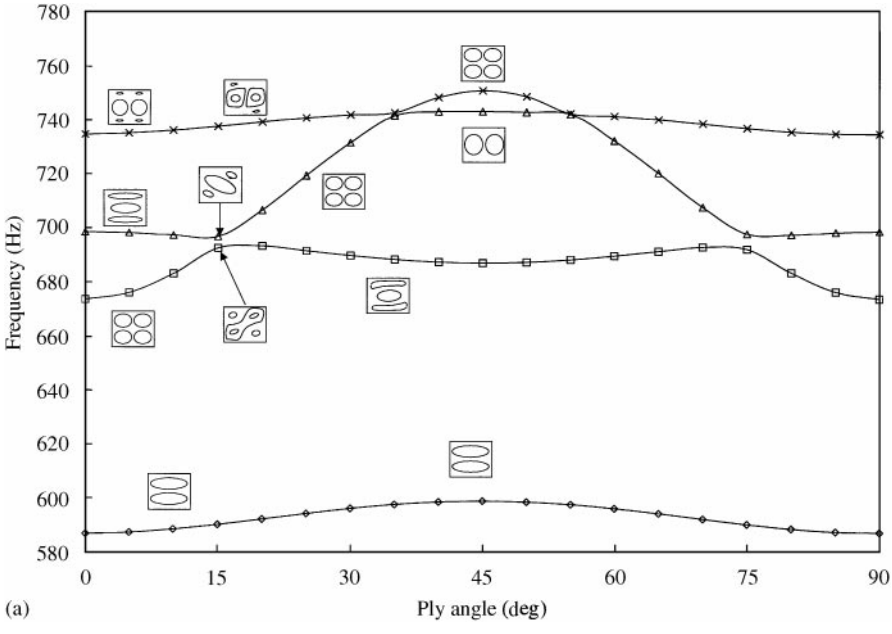

Figure 14. Effect of changing ply angle (middle two plies in the facing and backing skins) on the first four natural frequencies. Fully clamped along all four edges. (Key to natural frequency number: ◇: I, □, II, △: III, ×: IV): (a) $R_x = 3{\cdot}5$ m, $R_y = 1{\cdot}0$ m; (b) $R_x = 1{\cdot}2$ m, $R_y = 1{\cdot}0$ m; (c) $R_x = 3{\cdot}5$ m, $R_y = 0{\cdot}5$ m.

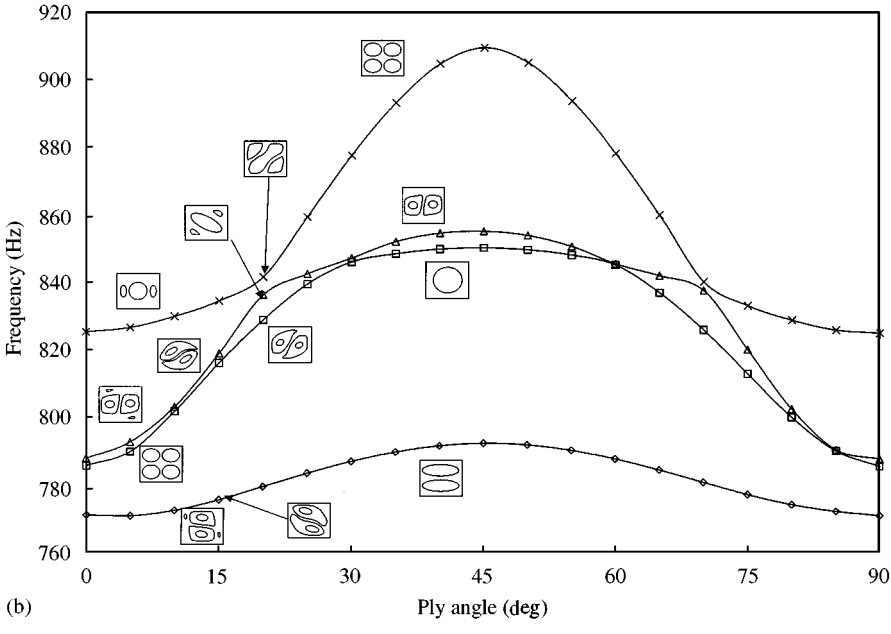

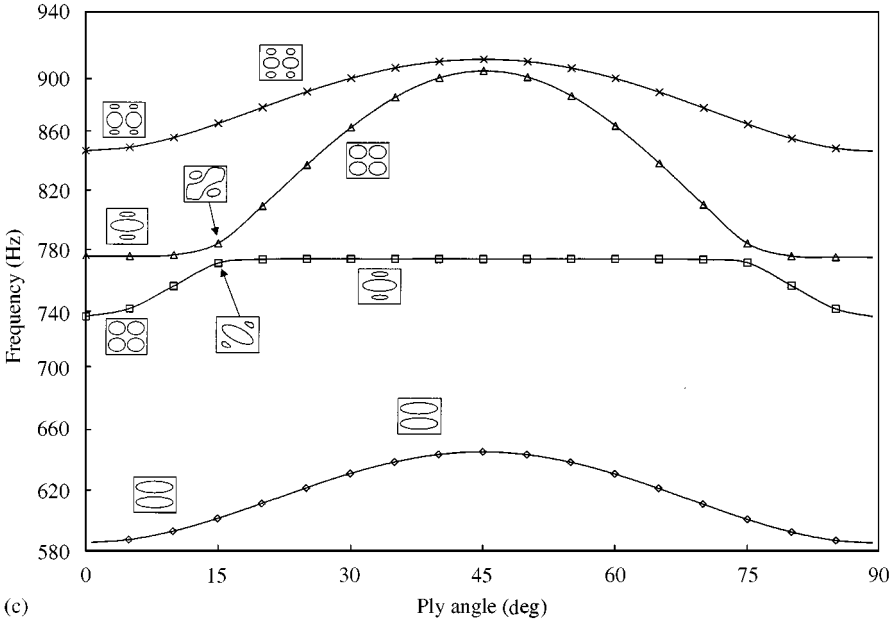

Figure 14. Continued.

- The natural frequency associated with the (1,2) mode of vibration appears to be relatively insensitive to changes in both the radius of curvature and ply orientation parameters for both the "pinned" and fully clamped boundary conditions.
- For the structures investigated, as the short-side radius of curvature is reduced below $R_y \approx 2.0$ m, the rate of change of frequency increased with decreasing

short-side radius for all long-side radii cases for both "pinned" and fully clamped boundary conditions. Therefore, the natural frequency appears to become more sensitive to changes in the parameters below $R_y \approx 2{\cdot}0$ m. From a practical point of view, considering the engine intake barrel panel, the smaller engine intakes would be more sensitive to changes in the geometry in terms of the radii of curvature compared to the larger engine intakes.

- The natural frequencies of vibration appear to be less sensitive to changes in the orthotropy of the core for the range of core shear modulii considered for both "pinned" and fully clamped boundary conditions.
- For the "pinned" boundary condition case, the high shear stiffness core is less sensitive to changes in orthotropy than the low shear stiffness core. This effect was reported by Jacobson [22] for studies carried out on flat sandwich panels with orthotropic cores and simply supported boundary conditions. In addition, the fundamental mode appears to be least sensitive to changes in the parameter for the $R_x = 1{\cdot}2$ m $\times R_y = 1{\cdot}0$ m case with "pinned" boundary conditions.
- A comparison between fully clamped and "pinned" boundary conditions shows that the former case results in an increased sensitivity to changes in the orthotropy, particularly for the high shear stiffness core.
- For "pinned" boundary conditions, the $R_x = 1{\cdot}2$ m $\times R_y = 1{\cdot}0$ m case shows the greatest sensitivity to changes in the ply orientation in terms of the fundamental natural frequency of vibration. For fully clamped boundary conditions, it is the $R_x = 3{\cdot}5$ m $\times R_y = 0{\cdot}5$ m case which results in the greatest overall change in the fundamental natural frequency with changing ply orientation. For both boundary conditions, the $R_x = 3{\cdot}5$ m $\times R_y = 1{\cdot}0$ m case shows the least sensitivity to changes in ply orientation in terms of the fundamental natural frequency.

6. SUMMARY

This paper has given details of one set of results from an ongoing study concerned with the response prediction of doubly curved composite sandwich panels. The manufacture of these panels has been discussed and experimental results are presented for the free vibration of three freely supported test panels. The development of a finite element model of the structures has been presented and validated using the experimental results. The model has demonstrated the use of shell elements to model a complex structure both in terms of construction and geometry, with excellent results being obtained compared with those obtained from experiment with freely supported boundary conditions.

Parameter studies have been carried out using the finite element model to investigate the effects of changing radii of curvature, orthotropy of the core, and ply orientation on the natural frequencies of vibration and a summary of the major sensitivites has been presented. The curve veering phenomenon has been observed when changing these parameters, particularly in the case of changing radii of curvature and ply orientation. As a certain parameter is varied, the system eigenfunctions are said to be coupled when this variation produces curve veering

[18]. It has been demonstrated that veering can occur in continuous systems as well as those represented by a discretized (approximate) model [18, 19], indicating that it is not always a result of the approximation method or errors in numerical calculation [17]. For the case presented here, it is not clear whether veering is a result of the approximation method used or is actually occurring in the physical system.

The present study has clearly demonstrated the effects of various design parameters on the first few natural frequencies of vibration of doubly curved composite honeycomb sandwich panels. By applying curve-fitting techniques such as least-squares to the curves presented in this paper, it should be possible to derive numerical formulae that would relate the fundamental frequencies of this type of panel to the design parameters such as the radius of curvature and orthotropic properties of the core. Although approximate, these formulae could be useful for the designer to outline the dynamic performance of a doubly curved sandwich panel.

ACKNOWLEDGMENTS

The programme of research is supported by the Engineering and Physical Sciences Research Council (EPSRC). The authors would also like to gratefully acknowledge the following for their advice and continuing support during this research programme; David Millar formerly of Short Brothers plc, Jacky Ridewood and Robin Phillips of Aerostructures (Hamble Group) Ltd, Jim Baker and Dave Edwards at the University of Southampton, and Professor Robin Langley for his helpful advice.

REFERENCES

1. J. Soovere 1984 *PhD Thesis, University of Southampton.* Dynamic response of acoustically excited stiffened composite honeycomb panels.
2. Engineering Sciences Data Unit *ESDU Design Guide Series* **1–6**. Vibration and acoustic fatigue.
3. D. Millar 1997 *Proceedings of the Sixth International Conference on Recent Advances in Structural Dynamics, ISVR, University of Southampton*, Vol. **2**, 995–1006. The behaviour of light weight honeycomb sandwich panels under acoustic loading.
4. D. J. Mead and A. J. Pretlove 1964 *Aeronautical Research Council.* R&M No. 3363. On the vibration of cylindrically curved elastic sandwich plates.
5. H. B. Zhou and G. Y. Li 1996 *Computers and Structures* **59**, 257–263. Free vibration analysis of sandwich plates with laminated faces using spline finite point method.
6. K. M. Ahmed 1971 *Journal of Sound and Vibration* **18**, 75–91. Static and dynamic analysis of sandwich structures by the method of finite elements.
7. J. Vaswani, N. T. Asnani and B. C. Nakra 1984 *Aeronautical Journal* **88**, 395–403. Vibration and damping analysis of doubly curved sandwich panels with viscoelastic core.
8. F. F. Rudder and H. E. Plumblee 1975 *Acoustics and Vibration Associates AFFDL-TR*-74-112. Sonic fatigue design for military aircraft.
9. J. W. Miles 1954 *Journal of the Aeronautical Sciences* **21**, 753–762. On structural fatigue under random loading.

10. A. Powell 1958 *The Journal of the Acoustical Society of America* **30**, 1130–1135. On the fatigue failure of structures due to vibrations excited by random pressure fields.
11. B. L. Clarkson 1968 *The Aeronautical Journal of the Royal Aeronautical Society* **72**, 1000–1010. Stresses in skin panels subjected to random acoustic loading.
12. R.G. White 1990 *Composite Structures* **16**, 171–192. Developments in the acoustic fatigue design process for composite aircraft structures.
13. J. N. Little and L. Shure 1992 *The MATH WORKS Inc*, chapter 2, 95. Signal processing toolbox. For use with MATLAB.
14. Ansys Inc., 201 Johnson Road, Houston, PA 15342–1300, U.S.A.
15. P. R. Cunningham and R. G. White 1990 *IMAC XVII*, *Proceedings of the* 17*th International Modal Analysis Conference*, 65–71. Free vibration of doubly curved composite honeycomb rectangular sandwich panels.
16. J. Soovere 1986 *Journal of Aircraft* **23**, 537–544. Random vibration analysis of stiffened honeycomb panels with beveled edges.
17. A. W. Leissa 1974 *Journal of Applied Mathematics and Physics* (*ZAMP*) **25**, 99–111. On a curve veering abberation.
18. N. C. Perkins and C. D. Mote Jr 1986 *Journal of Sound and Vibration* **106**, 451–463. Comments on curve veering in eigenvalue problems.
19. J. R. Kuttler and V. G. Sigillito 1981 *Journal of Sound and Vibration* **75**, 585–588. On curve veering.
20. P. T. Chen and J. H. Ginsberg 1992 *Journal of the Acoustical Society of America* **92**, 1499–1508. Modal properties and eigenvalue veering phenomena in the axisymmetric vibration of spheroidal shells.
21. M. Petyt 1971 *Journal of Sound and Vibration* **15**, 381–395. Vibration of curved plates.
22. M. J. Jacobson 1966 *The Shock and Vibration Bulletin* **35**, 9–14. Effects of orthotropic cores on the free vibration of sandwich plates.